JOURNAL OF GEOPHYSICAL RESEARCH, VOL. 105, NO. D8, PAGES 9949-9970, APRIL 27, 2000

Retrieving the vertical structure of the effective aerosol complex index of refraction from a combination of aerosol in situ and remote sensing measurements during TARFOX

J. Redemann,[1] R.P. Turco,[2] K.N. Liou,[2] P.B. Russell,[3] R.W. Bergstrom,[1] B. Schmid,[1] J.M. Livingston,[4] P.V. Hobbs,[5] W.S. Hartley,[5] S. Ismail,[6] R.A. Ferrare,[6] and E.V. Browell[6]

Abstract. The largest uncertainty in estimates of the effects of atmospheric aerosols on climate stems from uncertainties in the determination of their microphysical properties, including the aerosol complex index of refraction, which in turn determines their optical properties. A novel technique is used to estimate the aerosol complex index of refraction in distinct vertical layers from a combination of aerosol *in situ* size distribution and remote sensing measurements during the Tropospheric Aerosol Radiative Forcing Observational Experiment (TARFOX). In particular, aerosol backscatter measurements using the NASA Langley LASE (Lidar Atmospheric Sensing Experiment) instrument and *in situ* aerosol size distribution data are utilized to derive vertical profiles of the "effective" aerosol complex index of refraction at 815 nm (i.e., the refractive index that would provide the same backscatter signal in a forward calculation on the basis of the measured *in situ* particle size distributions for homogeneous, spherical aerosols). A sensitivity study shows that this method yields small errors in the retrieved aerosol refractive indices, provided the errors in the lidar-derived aerosol backscatter are less than 30% and random in nature. Absolute errors in the estimated aerosol refractive indices are generally less than 0.04 for the real part and can be as much as 0.042 for the imaginary part in the case of a 30% error in the lidar-derived aerosol backscatter. The measurements of aerosol optical depth from the NASA Ames Airborne Tracking Sunphotometer (AATS-6) are successfully incorporated into the new technique and help constrain the retrieved aerosol refractive indices. An application of the technique to two TARFOX case studies yields the occurrence of vertical layers of distinct aerosol refractive indices. Values of the estimated complex aerosol refractive index range from 1.33 to 1.45 for the real part and 0.001 to 0.008 for the imaginary part. The methodology devised in this study provides, for the first time, a complete set of vertically resolved aerosol size distribution and refractive index data, yielding the vertical distribution of aerosol optical properties required for the determination of aerosol-induced radiative flux changes.

1. Introduction

The low confidence in estimates of aerosol-induced changes in the Earth's radiation balance is caused by the highly nonuniform spatial and temporal distribution of tropospheric aerosols on a global scale (because of their heterogeneous sources and short lifetimes) [*Charlson et al.*, 1992; *Penner et al.*, 1994; *Haywood and Ramaswamy*, 1998]. Nevertheless, recent studies have shown that the inclusion of aerosol effects in model calculations can improve the agreement with the observed spatial and temporal temperature distributions [*Hansen et al.*, 1995; *Tett et al.*, 1996].

In light of the short lifetimes of aerosols, the exploration of their global distribution with space-borne sensors seems to be a necessary approach. Until recently, satellite measurements of tropospheric aerosols have been qualitative in nature and did not provide the full set of information required for a determination of their radiative effects. Ideally, such information should include the derived aerosol properties [*Toon*, 1994], i.e., the aerosol optical depth, single-scattering albedo, and asymmetry factor (phase function), all of which appear in the equations of radiative transfer. In principle, the derived aerosol properties can be determined from the fundamental aerosol properties, such as size distribution, chemical composition, and wavelength-dependent optical constants. To obtain these aerosol properties on a global basis, a variety of large-scale measurement programs sponsored by national (NASA, National Oceanic and Atmospheric Administration (NOAA), National Science Foundation (NSF)) and international (World Meteorological Organization (WMO)) organizations are being carried out. These programs include but are not limited to the Global Backscattering Experiment (GLOBE), Atmospheric Boundary Layer Experiments (ABLE), Transport and Atmospheric Chemistry (TRACE), Pacific Exploratory Mission (PEM), Tropospheric Aerosol Radiative Forcing Observational Experiment (TARFOX), and Aerosol Characterization Experiment (ACE).

[1] Bay Area Environmental Research Institute, San Francisco, California.
[2] Department of Atmospheric Sciences, University of California, Los Angeles.
[3] NASA Ames Research Center, Moffett Field, California.
[4] SRI International, Menlo Park, California.
[5] Department of Atmospheric Sciences, University of Washington, Seattle.
[6] NASA Langley Research Center, Hampton, Virginia.

Paper number 1999JD901044.
0148-0227/00/1999JD901044$09.00

In this paper we describe work carried out with the TARFOX data set regarding the vertical structure of the aerosol index of refraction, while *Redemann et al.* [this issue] will make use of the results obtained here to calculate the vertical structure of the aerosol radiative forcing (i.e., the aerosol-induced change in the net shortwave irradiance due to the direct interaction with solar radiation). TARFOX was conducted July 10-31, 1996, to study the plume of pollutant haze emanating from the continental United States over the western Atlantic Ocean. The time and location of TARFOX were chosen based on a statistical analysis of satellite data, which showed a high probability of observing episodic anthropogenic aerosol plumes (under relatively cloud-free conditions) off the U.S. east coast in July [*Russell et al.*, 1999a].

The main idea for the TARFOX data analysis presented in this paper is analogous to the approach taken by *Redemann et al.* [1998a] for the analysis of data collected during the Pacific Exploratory Mission (PEM) West B, namely, to derive vertical profiles of the "effective" aerosol complex index of refraction from a set of *in situ* aerosol size distribution measurements and lidar aerosol backscatter data (i.e., the refractive index which would provide the same backscatter signal in a forward calculation on the basis of the measured *in situ* size distributions and homogeneous, spherical aerosols). The aerosol complex index of refraction together with the particle size determines the aerosol optical properties, thereby affecting aerosol impact on climate [e.g., *Sokolik and Toon*, 1999; *Jacobson*, 2000]. Especially when large particles are abundant, the derived aerosol optical properties show a strong dependence on the imaginary part of the refractive index. For the TARFOX radiative forcing studies based on the aerosol refractive index results described here, *Redemann et al.* [this issue] report a change of 26-32% in the aerosol-induced radiative flux change at the top of the atmosphere (TOA) in response to a 5% change in the real part of the aerosol complex index of refraction. They compute a change of only 5% in TOA aerosol radiative forcing due to a 20% change of the imaginary refractive index. Likely, this lack of sensitivity to the imaginary index of refraction is caused by the relatively small absolute values of this quantity derived here and is not representative of other aerosol types.

Despite its relative importance, there have been only a few attempts to estimate the aerosol index of refraction from its optical properties. *Takamura and Sasano* [1992] report a study of stratospheric aerosols in which the combination of a ground-based lidar system with sunphotometer and optical particle counter data was used to estimate the range of a column-averaged aerosol index of refraction. *Takamura et al.* [1994] focused on the retrieval of the imaginary part for tropospheric aerosols after assuming a real part, while *Ferrare et al.* [1998a, b] obtained an estimate of the real part of the aerosol refractive index from a combination of scanning Raman lidar with simultaneous airborne aerosol *in situ* size distribution measurements. In this sense, the work of *Ferrare et al.* [1998a, b] most closely resembles the approach taken here.

In this study we will attempt to determine both the real and the imaginary parts of the aerosol complex index of refraction. Moreover, the vertical structure of the aerosol index of refraction will be estimated, based on the assumption that the aerosol refractive index is constant within vertical layers of the atmosphere. The merit of this technique is that it provides, for the first time, vertically resolved aerosol optical properties. Knowledge of column-integrated aerosol properties may make possible the calculation of aerosol-induced radiative flux changes at the top/bottom of the atmosphere (or at the top/bottom of an aerosol layer). Vertically resolved information on aerosol optical properties and radiative effects, however, has the capability of greatly improving our understanding of aerosol effects on atmospheric temperature profiles, surface temperatures,

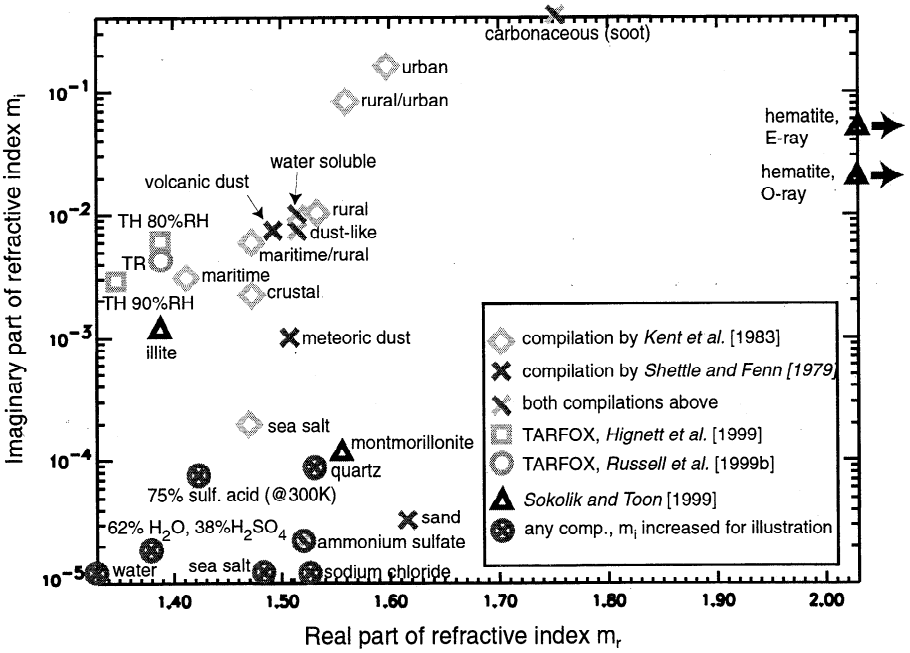

Figure 1. The 815 nm aerosol refractive index regime considered for the TARFOX case studies. Published values from the literature are indicated. For illustration purposes the imaginary parts of all data points in the bottom left-hand corner have been increased to fall into the plotting range.

large-scale circulation patterns, and the redistribution of trace species through convective processes. Indeed, *Redemann et al.* [this issue], using the refractive index and *in situ* size distribution data derived in this study, carry out the first detailed calculations of the vertical structure of aerosol-induced changes in the Earth's radiation field based on observations. The Fu-Liou broadband radiative flux model is employed for this purpose [*Fu and Liou*, 1992, 1993].

Figure 1 shows values of the aerosol complex index of refraction at 815 nm for a variety of aerosol types and materials [*Shettle and Fenn*, 1979; *Kent et al.*, 1983; P. Hignett, personal communication, 1998; *Russell et al.*, 1999b; *Sokolik and Toon*, 1999]. The imaginary parts of the data points marked with circled crosses in the bottom left-hand corner of Figure 1 have been increased from their original value for illustration purposes. The original values are all in the range of 10^{-6} to 10^{-7}. Figure 1 also represents the regime considered for the estimate of the aerosol index of refraction in this paper. The refractive index regime was not extended to imaginary parts smaller than 10^{-5}, because the aerosol backscatter and extinction for typical particle size distributions measured during TARFOX are not sensitive to imaginary refractive indices smaller than this value [*Redemann*, 1999]. Hence, in general, optical measurements of aerosol backscatter and extinction do not contain any information on aerosol imaginary refractive indices smaller than ~ 10^{-5} (for real parts smaller than ~1.6).

The remote sensing data utilized in this work consist of aerosol scattering ratio (backscatter) profiles measured using the NASA Langley airborne LASE (Lidar Atmospheric Sensing Experiment) instrument aboard the NASA ER-2 aircraft [*Browell et al.*, 1996]. *In situ* aerosol size distributions are taken from a variety of optical probes employed on the University of Washington (UW) C-131A aircraft [*Hobbs*, 1999], while aerosol optical depths at four wavelengths (380.1, 450.7, 525.3, and 1020.7 nm) are derived from measurements using the six-channel NASA Ames Airborne Tracking Sunphotometer (AATS-6) [*Matsumoto et al.*, 1987; *Russell et al.*, 1999b], which was also mounted on the C-131A aircraft.

2. Estimating Vertical Profiles of the Effective Aerosol Complex Index of Refraction

2.1. Approach

During TARFOX the instruments that provide the data for the refractive index estimation scheme were not located on the same aircraft. The *in situ* particle size distribution and sunphotometer data were obtained from instruments aboard the University of Washington (UW) C-131A aircraft, while the LASE lidar system supplying the aerosol backscatter profiles was situated aboard the NASA ER-2 aircraft. Consequently, a careful screening of the data sets to find the times and locations of maximum coincidence between the measurements aboard the two aircraft was necessary.

Once the time periods with sufficient coincidence between the ER-2 and the UW C-131A measurements were identified, the analysis of the TARFOX data had distinct advantages over the PEM West B analysis [*Redemann et al.*, 1998a, b]. For instance, the aerosol optical depth measurements from AATS-6 could be successfully integrated into the refractive index retrieval scheme, thereby providing a more complete picture of the vertical variations of the aerosol index of refraction.

This section will describe the synthesis of the data from the aerosol *in situ* and sunphotometer package aboard the UW C-131A with the lidar-derived aerosol backscatter data collected by the LASE instrument aboard the ER-2 aircraft. Figure 2 shows the basic setup for the comparison of the lidar-derived aerosol backscatter profile to the backscatter profiles calculated using the *in situ* size distribution data.

2.2. *In situ* Size Distribution Data Analysis

The most comprehensive aerosol instrumentation package in the TARFOX field campaign was situated aboard the University of Washington C-131A research aircraft. The data obtained from this measurement platform included the concentration of condensation nuclei (CN), cloud condensation nuclei (CCN), aerosol composition and size distribution, total scattering, hemispheric backscattering and absorption coefficients, total (graphitic plus organic) carbon, aerosol hygroscopic growth factor for scattering, and a variety of cloud/fog properties using *in situ* instruments. In addition to the *in situ* measurements aboard the UW C-131A aircraft, solar beam transmission measurements were carried out with the NASA Ames Airborne Tracking Sunphotometer (AATS-6) yielding aerosol optical depths at 380.1, 450.7, 525.3, and 1020.7 nm.

The *in situ* particle size distribution measurements were obtained from a variety of instruments aboard the UW C-131A aircraft. For the forward calculation of aerosol backscattering in this paper we used aerosol size distribution measurements from three different instruments: the passive cavity aerosol spectrometer probe (PCASP), which measures aerosols in the radius range of 0.05 to 1.5 μm, the forward scattering spectrometer probe 300 (FSSP-300), which covers the radius range 0.15 to 10 μm, and the FSSP-100, which detects particles in the radius range 1.0 to 23.5 μm. All these radius ranges are the nominal ranges given by the instrument manufacturer (PMS, Boulder, Colorado). However, as pointed out by numerous investigators [*Pueschel et al.*, 1990; *Baumgardner et al.*, 1992; *Cutten et al.*, 1996], aerosols in the atmosphere likely possess a different refractive index from the particles used to calibrate these instruments.

The following adjustments were made to account for calibration differences. Both FSSP probes measure particles under ambient conditions, while the PCASP instrument was operated with a deicing heater, which reduced the relative humidity inside the PCASP to ~10-40%. The PCASP therefore measured a "dry" particle size distribution, and any adjustment to the particle size ranges has to account for the difference between the refractive index of the dry TARFOX aerosol and that of the calibration particles. Based on an assumed mean dry aerosol refractive index of $1.487 - 0.016i$ (deduced from TARFOX-averaged chemical composition measurements), the PCASP size ranges can be recalculated, resulting in 15 radius ranges from 0.0525 to 3.36 μm. The UW aerosol measurement group has run a number of in-house calibration studies for the FSSP instruments. Summarizing their results, the FSSP-100 has been shown to size ambient TARFOX-like particles properly to within two size channels. However, the FSSP-300 often lacks accuracy in particle sizing, especially for particles in the upper radius range of the instrument. In spite of this there seemed to be no inflation of the small-radius channels of the FSSP-300 instruments relative to other instruments in the TARFOX field campaign. In an attempt to account for the different refractive index of the TARFOX aerosol from the calibration particles, we

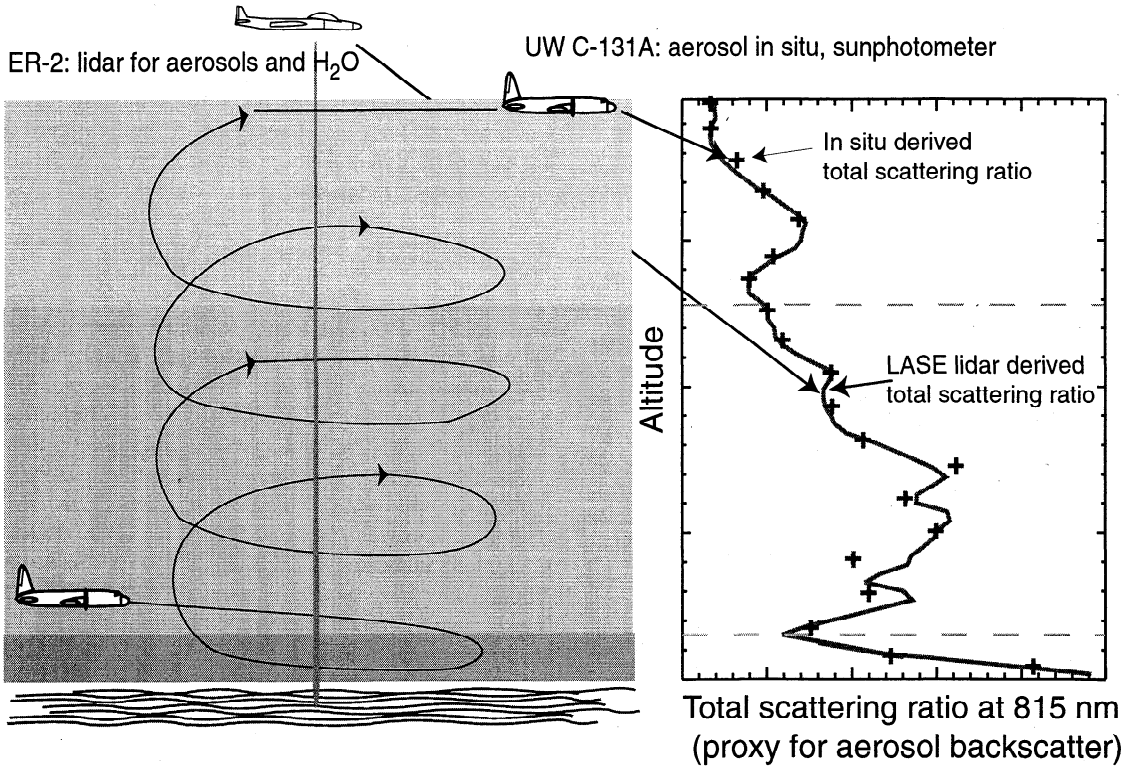

Figure 2. Approach: during local UW C-131A aircraft ascents, record the *in situ* particle size distribution, bin into 40- to 60-s averages and forward calculate aerosol backscatter profile at the Lidar Atmospheric Sensing Experiment (LASE) wavelength of 815 nm (see discrete values in right-hand panel). At the same time, measure lidar backscatter ratio profiles with the NASA Langley LASE lidar system aboard the ER-2 aircraft (solid line in right-hand panel).

rebinned the nominal 30 channels of the FSSP-300 into 18 radius classes from 0.21 to 11.84 μm, based on a recalculated FSSP-300 response curve for aqueous sulfuric acid particles. While the composition and refractive indices of the aerosols may have varied considerably, the sulfuric acid calibration is likely to be closer to reality. In the actual refractive index retrieval scheme (see sections 2.5) the impact of the FSSP-300-derived particle sizes on the retrieved refractive indices will be investigated. No rebinning was applied to the FSSP-100 data, because of its better performance in the calibration studies and because of the larger size ranges for each of the instrument channels, which reduces any erroneous sizing effects.

Hartley et al. [this issue] have used nephelometer measurements and independently measured humidification factors to achieve closure with the sunphotometer-derived aerosol optical depth at 450 nm. Their comparison shows that the *in-situ*-derived aerosol optical depth is generally less than the sunphotometer-derived aerosol optical depth by about 12%. This difference could be due to the loss of some large aerosols in the intake tubes leading to the nephelometer or, as *Hartley et al.* [this issue] speculate, might be caused by a possible volatilization of some organic compounds during heating in the sample airstream.

To avoid problems associated with a possible humidification of the PCASP dry aerosol measurements and to minimize errors that might result from the inaccurate sizing of the particles by the FSSP instruments, the following steps were taken in the synthesis of composite aerosol size distributions from the three instruments. (1) We used the PCASP dry aerosol measurements in the radius range 0.0525 to 0.2 μm, where we found the effect of particle dehydration on forward calculated aerosol backscattering for typical TARFOX aerosol size distributions to be minimal. (2) We utilized the FSSP-300 data in the overlap region (0.2 to 1.6 μm) of the PCASP and the FSSP-300 to avoid humidification calculations of the PCASP measurements. (3) We used the FSSP-100 data in its overlap region with the FSSP-300 (>1.6 μm), since the FSSP-100 has a sampling volume that is a factor of ~4 larger than the sampling volume of the FSSP-300. Figure 3 shows examples of composite aerosol size distributions from the three instruments discussed here.

For the purpose of calculating the aerosol backscattering and extinction from the *in situ* aerosol size distribution data, the discrete values in the aerosol number concentration measurements were connected using power-law functions (i.e., straight lines in a log-log plot). Additionally, the size distributions were analytically extended to a radius of 20 μm by fitting a lognormal distribution to the large-particle mode of the size distribution composites. In general, this extension increased aerosol backscattering by 1-8% (with a maximum increase of 15%) and had negligible impact on particle size distributions, which already contained particles in the radius range greater than 5 μm.

2.3. LASE Lidar Data Analysis

A total of 72 hours of research data were gathered with the UW C-131A platform during the TARFOX experiment. Seven sets of profile measurements beneath the ER-2 aircraft were obtained. The ER-2 aircraft carried the NASA Langley DIAL (Differential Absorption Lidar) system developed for the LASE

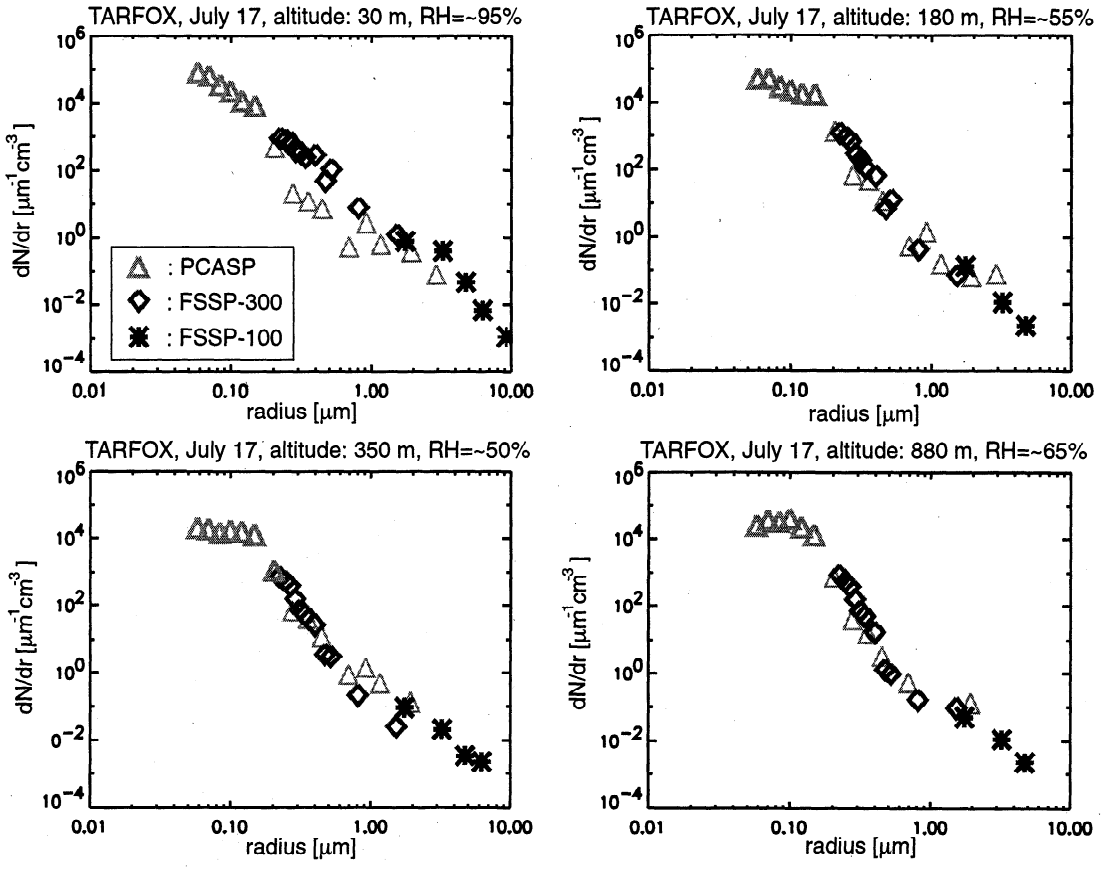

Figure 3. Examples of composite particle size distributions, using three different particle size spectrometers: a passive cavity acrosol spectrometer probe (PCASP) (triangles), a forward scattering spectrometer probe (FSSP-300) (diamonds), and an FSSP-100 (asterisks). The data points used for subsequent calculation of optical parameters are shown in bold symbols.

campaign. The LASE instrument is the first autonomous DIAL system for the measurement of water vapor, aerosols, and clouds in the troposphere [*Browell et al.*, 1996]. The laser source is a Ti:Sapphire power oscillator which is pumped by a frequency doubled Nd:Yag laser [*Moore et al.*, 1996]. The Ti:Sapphire laser has a tuning range, which includes the 813 to 819 nm wavelength region required for the differential absorption measurement of the 815 nm water vapor absorption line. A 38-cm-diameter telescope collects the backscattered signals and directs them to the detection unit. During TARFOX the LASE instrument collected data at a rate of 5 Hz.

The measurements of the LASE instrument have been intercompared with many different *in situ* and remote water vapor measurements. These intercomparisons have yielded a measurement accuracy of better than 6% or 0.01 g/kg, whichever is greater, across the entire troposphere [*Browell et al.*, 1996; *Ismail and Browell*, 1998].

The aerosol backscatter signal of the off-line wavelength of the LASE [*Ferrare et al.*, 1998c; *Ferrare et al.*, this issue] has been archived at the NASA Langley Distributed Active Archive Center (DAAC) in the form of the total scattering ratio R defined as

$$R(z)=\frac{\beta_{\mathrm{aer}}(z)+\beta_{\mathrm{mol}}(z)}{\beta_{\mathrm{mol}}(z)}=\frac{\beta_{\mathrm{aer}}(z)}{\beta_{\mathrm{mol}}(z)}+1, \tag{1}$$

where β_{aer} and β_{mol} are the aerosol and molecular backscatter coefficient, respectively.

In the present analysis the LASE lidar system was situated on the high-altitude ER-2 aircraft, usually flying at an altitude of 17-20 km. This permits the "anchoring" of the lidar profile at an altitude that can be assumed to be relatively aerosol free, with a total scattering ratio of 1.05. The second assumption in the processing of the LASE lidar data was that the lidar ratio (i.e., the ratio of aerosol extinction to backscatter) was 60 sr [*Ferrare et al.*, this issue], as indicated by independent Raman lidar measurements at Wallops Island, Virginia. This value can be tested by dividing the aerosol optical depth derived from the Ames sunphotometer by the altitude-integrated lidar-derived aerosol backscatter, thus yielding an altitude-integrated extinction-to-backscatter ratio:

$$\bar{g}=\frac{\tau_{\mathrm{sp}}}{\int_0^{z_{\max}}\beta_{\mathrm{aer}}(z)dz}, \tag{2}$$

where $\beta_{\mathrm{aer}}(z)$ is the lidar-derived aerosol backscatter coefficient, and τ_{sp} is the sunphotometer-derived aerosol optical depth. Although the values of $\bar{g}$ generally agreed with the value of 60 sr to within 10-20%, the lidar backscatter values are likely subject to larger errors at altitudes that are farther away from the anchoring point.

The LASE data obtained during TARFOX are archived in the form of 6-s averaged total scattering ratio profiles. At typical ER-2 flight speeds a time period of 6-s is roughly equivalent to a

horizontal distance of 1 km. Because the ascents of the UW C-131A were flight spirals with diameters of the order of 10 km, a careful selection of the LASE profiles, which are to be used for the refractive index retrieval, is necessary.

For this purpose, we compare all the 6-s scattering ratio profiles in a time period of ± 5 min of the overpass of the ER-2 flight track with the UW C-131A ascent location to first-guess scattering ratio profiles derived from the *in situ* aerosol size distribution measurements under the assumption of a constant aerosol index of refraction (see Figure 4). Although the magnitudes of the *in situ* scattering ratios thus derived are likely to be different from the lidar-scattering ratios, the altitude variation is usually preserved. In other words, a minimum in the first estimate of the *in situ* scattering ratio profile is still going to be a local minimum once the correct aerosol index of refraction is prescribed. Figure 4 shows six nonconsecutive profiles, illustrating this kind of comparison. Note the poor agreement in the comparison shown in the scattering ratio profiles at 19:06:19, which would result in exclusion of this lidar profile from any further data processing.

2.4. Ames Sunphotometer Data Analysis

During the TARFOX field campaign the six-channel NASA AATS-6 [*Matsumoto et al.*, 1987; *Russell et al.*, 1999b] yielded the aerosol optical depth at 380.1, 450.7, 525.3, and 1020.7 nm. During ascents of the UW C-131A aircraft these data provided useful information on the vertical variation of aerosol extinction.

In an atmosphere that is horizontally homogeneous and time invariant, the aerosol optical depth measured during an aircraft ascent would be monotonically decreasing with increasing altitude, since the aerosol optical depth is simply the altitude integral of aerosol extinction. However, in the real atmosphere, a subvisible/visible cloud or contrail that intercepts the sunphotometer-to-Sun path causes an abrupt increase in the aerosol optical depth. Such increases can occur when sunphotometer altitude is increasing. Additionally, aerosol plumes and patches can cause analogous, though less abrupt, increases with aircraft altitude. Figure 5a shows an example of a four-wavelength sunphotometer optical depth profile that contains such an "optical depth anomaly" at an altitude of ~2 km. For the calculation of the total column aerosol optical depth these anomalies are of no consequence, since the optical depth of the entire aerosol layer can be simply calculated from the difference of the aerosol optical depths at the bottom and at the top of the layer. In this work, however, use will be made of the aerosol optical depth in several distinct layers along the profile. Therefore these "anomalies" have to be filtered from the raw sunphotometer data to improve the accuracy of the deduced aerosol optical depths in these layers.

For this purpose we devised a simple routine that sorts through the raw sunphotometer optical depth data profiles from bottom to top and suppresses any data points for which the optical depth at any of the four wavelengths increases with altitude. These filtered data are shown in Figure 5a as thin solid lines.

Also shown in Figure 5b are the optical depths for three distinct layers derived from differencing the filtered data at the

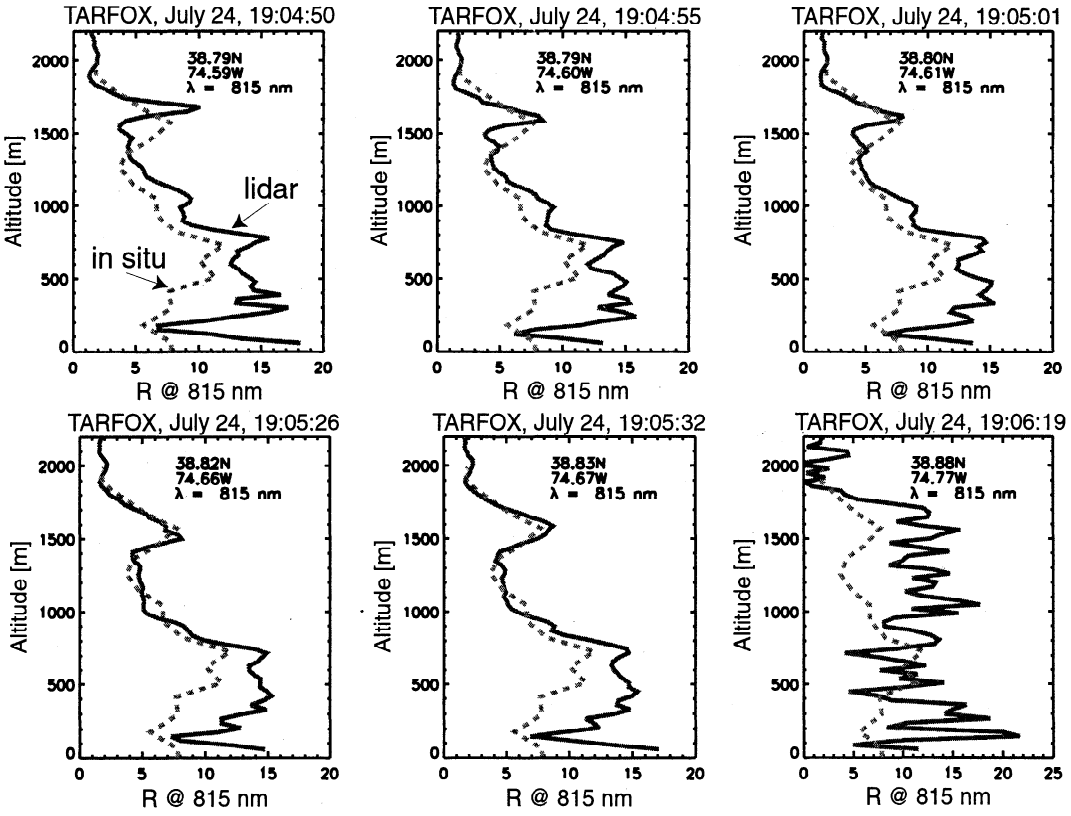

Figure 4. Examples of comparisons between 6-s average LASE scattering ratio profiles (solid lines) as archived in the NASA Langley DAAC (Distributed Active Archive Center) and *in-situ*-derived scattering ratio profiles (dashed lines) using best guess aerosol refractive indices. Note that these profiles are not in consecutive order but are shown to illustrate the data screening process.

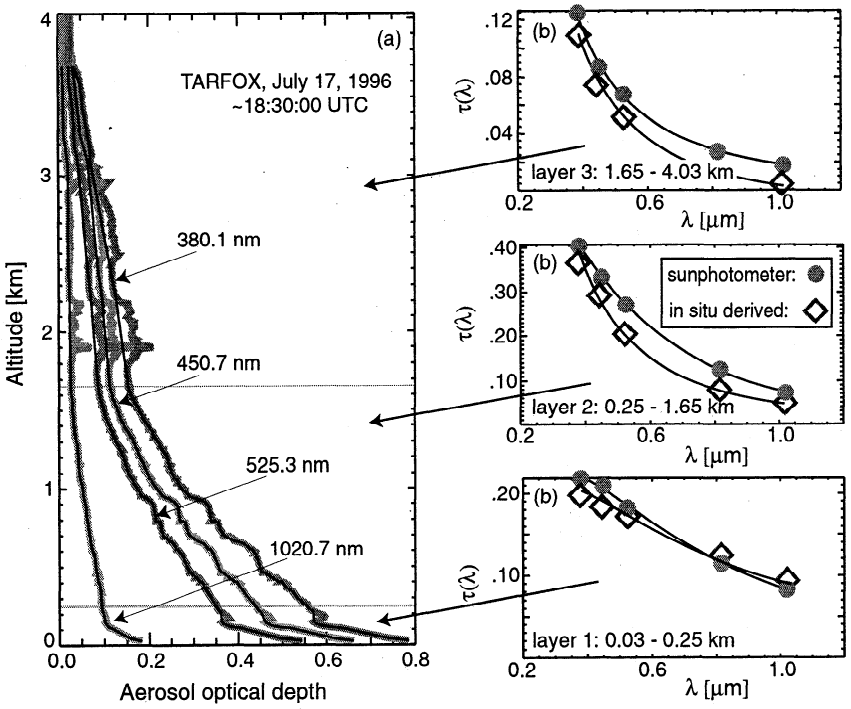

Figure 5. (a) Sunphotometer-derived aerosol optical depth measurements on July 17, 1996. The gray lines represent the raw data at the indicated wavelengths, while the thin solid black lines represent the filtered data to suppress optical depth inhomogeneities. (b) Aerosol optical depths spectra for distinct layers, achieved by differencing the filtered curves in Figure 5a at the indicated altitudes.

indicated altitudes. Note that this differencing must produce positive optical depths (as is physically reasonable) as a result of the monotonic behavior of the filtered sunphotometer data. The sunphotometer-measured aerosol optical depths at 380.1, 450.7, 525.3, and 1020.7 nm can be used to determine the aerosol optical depth at a different wavelength. For this purpose an equation of the form

$$\ln\tau = a + b\ln\lambda + c\ln^2\lambda \tag{3}$$

was fitted to individual sunphotometer-derived aerosol optical depth spectra, enabling the calculation of the aerosol optical depth at the LASE wavelength (815 nm). In (3), a, b, and c are fitting parameters that need to be determined individually for each optical depth spectrum. Figure 5b also contains examples of curves fitted to the discrete sunphotometer optical depth spectra with the functional form given in (3).

2.5. Advanced Refractive Index Retrieval Technique

The LASE lidar-derived scattering ratio profiles do not contain any information from the *in situ* aerosol size distribution data and are, consequently, fixed for the purpose of this study. Therefore the task of retrieving the aerosol index of refraction is reduced to finding the aerosol index of refraction that best reproduces the lidar-derived scattering ratio profile when forward calculated from the *in situ* aerosol size distribution data. Note that if there were only one aerosol size distribution and one lidar-derived scattering ratio value, respectively, this would clearly be an ill-posed problem. The ill-posed nature of the problem arises from the attempt to deduce both the real part m_r and the imaginary part m_i of the complex aerosol refractive index from just one set of measurements. However, assuming that the complex index of refraction is constant over a certain vertical distance within the atmosphere adds additional constraints (analogous to the technique developed by *Redemann et al.* [1998a, b]). In other words, a minimum of two lidar-derived scattering ratios and two *in situ* particle size distributions, respectively, together with the assumption that the aerosol refractive index is the same for both size distributions, is sufficient to retrieve that aerosol refractive index.

The mathematical formulation of this problem is the minimization of the absolute value of the relative difference Δ between the lidar-derived scattering ratios R_{lidar} and the *in-situ*-derived scattering ratio R_{is} for the sum of N points in a given layer:

$$\Delta(m_r,m_i) = \frac{1}{N}\sum_{j=1}^{N}\frac{\left|R_{\mathrm{is}}[z_j,n(z_j),m_r,m_i] - R_{\mathrm{lidar}}(z_j)\right|}{R_{\mathrm{lidar}}(z_j)}. \tag{4}$$

Here j counts the number of data points at which the above difference can be evaluated (i.e., the number of size distribution measurements within the given layer, minimum 2), and $n(z_j)$ is the *in-situ*-measured particle size distribution at altitude z_j. This minimization is carried out independently for every layer, in which a different index of refraction is expected. Figure 6 shows an example of a contour plot of the quantity Δ as a function of the real and the imaginary parts of the aerosol refractive index, with the location of its minimum denoted by a circle. For the purpose of calculating the *in situ* scattering ratio R_{is} from the *in situ* aerosol size distributions, a standard Mie code [*Bohren and Huffman*, 1983] and formulations of the molecular backscattering coefficient from *Measures* [1984] were used. The atmospheric

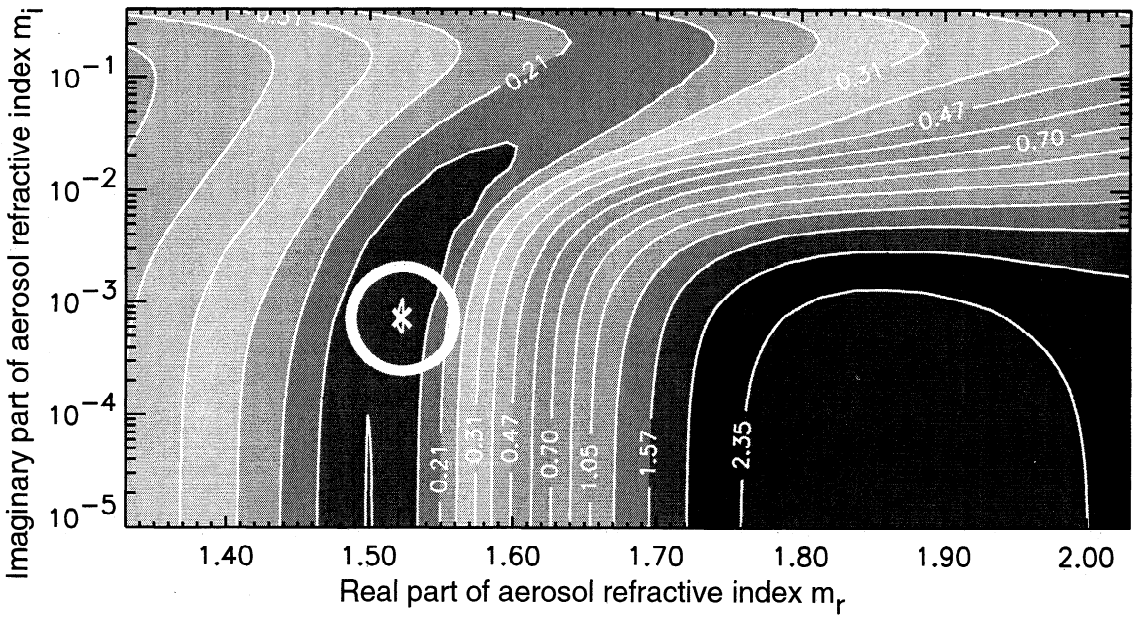

Figure 6. Example of a contour plot of Δ as a function of the real and imaginary parts of the aerosol refractive index. The circles mark the location of the minimum in Δ, indicating the best fit aerosol refractive index.

density profile required for these calculations was derived from *in situ* measurements of temperature and pressure aboard the UW C-131A aircraft.

The fundamental difference from the work of *Redemann et al.* [1998a], where the best match refractive index was retrieved by testing a set of seven discrete complex refractive indices only, is that in the present study the refractive index is estimated from a semicontinuous set of refractive indices in the domain $1.33 < m_r < 2.03$ and $10^{-5} < m_i < 0.4$. By semicontinuous we mean that the refractive index domain is subdivided into a much finer grid of discrete values both in the real and in the imaginary parts. Aerosol optical properties (backscatter and extinction) are specified in a look-up table with a resolution of 30 linear steps in the real part and 50 geometrically divided steps in the imaginary part. This subdivision, and the precalculation of the aerosol backscatter coefficient as a function of the refractive index for all the size distributions in a given layer, is necessary to improve the speed of the refractive index retrieval routine.

The task of estimating the aerosol refractive index that provides the best match between the lidar-derived aerosol backscatter profile and the backscatter profile calculated using the *in situ* size distributions is then reduced to finding the minimum of Δ as a function of the real and the imaginary parts of the aerosol refractive index in a simple look-up table approach. This technique circumvents the necessity to recalculate the aerosol backscatter as a function of the aerosol complex index of refraction for each refractive index estimation run.

At the same time, this technique poses the problem of finding the minimum of a two-dimensional function on a finite grid. Depending on the shape of the minima in the contour plots of the quantity Δ, the grid itself can introduce errors in the retrieved complex refractive index (see Figure 6). For example, if the minimum is aligned vertically (parallel to lines of constant m_i), the information content regarding the imaginary part of the index of refraction m_i is limited. Indeed, we found that at a resolution of the complex refractive index domain of 20 steps in the real and 40 steps in the imaginary part, the retrieved value of m_i frequently varied from its correct value by more than one grid cell. Upon implementing a search routine at a finer resolution (30 x 50), this phenomenon occurred less frequently, which made us decide in favor of the computationally more extensive resolution.

We further investigated whether the selection of a different norm from (the linear norm in) equation (4) leads to the retrieval of different minima in Δ. For example, a norm of the order of p has the form

$$\Delta(m_r,m_i)=\frac{1}{N}\left[\sum_{j=1}^{N}\left|R_{\mathrm{is}}[z_j,n(z_j),m_r,m_i]-R_{\mathrm{lidar}}(z_j)\right|^p\right]^{1/p}, \quad (5)$$

with $p = 1, 2, \ldots, \infty$. For the case studies described in section 3 we found no variation of the minima in Δ determined with (4) from those calculated using (5) and $p = 1$ or 2, indicating the validity of the retrieved minima.

The difficulties described above are inherent problems of the method of finding a minimum of a function of two variables on a finite grid [cf. *Kuze and Chance*, 1994]. Given the measurement uncertainties in the input scattering ratios R_{is} and R_{lidar}, we conclude that a more sophisticated method to determine the minima in Δ is not required, since the error in the retrieved best fit aerosol index of refraction introduced by the grid search method itself is comparably small (see sections 2.6).

2.6. Sensitivity Studies

For the purpose of testing the performance of the new refractive index retrieval routine a total of 12 sensitivity studies were carried out. These 12 case studies were intended to simulate all possible sources of errors and to quantify the errors introduced by the grid search method itself (see section 2.5). To test the performance, an actual profile of measured TARFOX aerosol size distributions was utilized to synthesize a lidar signal on the premise of three different layers of distinct aerosol refractive

indices. In the most fundamental test of the routine, without any errors in either the *in situ* aerosol size distributions or the lidar signal, the input refractive indices should be retrieved exactly with a value of $\Delta = 0$. In subsequent cases we altered the *in situ* aerosol size distributions to simulate measurement errors and/or added errors in the lidar signal. The case studies and the retrieved refractive indices are given in Table 1. They can be divided into cases where (1) the input refractive indices are slightly offset from the discrete values of the refractive indices in the search grid (cases 2-4), (2) the lidar data are subject to a systematic error (cases 5-8), (3) the measured aerosol size distributions are underestimated by a factor of 20% in radius (case 9), and (4) the input lidar data are subject to a random error (cases 10-12). The random errors in case studies 10-12 are generated by a normally distributed number generator (absolute values of the average relative errors (∅) are also given in Table 1).

Summarizing the results in Table 1, the refractive index retrieval routine performs well, when the errors are random in nature (cases 10-12) or small in general (cases 2-4, 5, and 10). However, when the errors in the input lidar data are systematic and greater than 10% (cases 6-8), the refractive indices retrieved represent this circumstance accordingly. For example, an overestimate of the lidar-derived aerosol backscatter by 20% translates into an overestimate of the real part of the refractive index by about 0.06, since the refractive index estimation routines tries to contribute more backscattering to the same aerosol size distributions. Case study 9 shows the impact of an underestimate of 20% in the FSSP-300 particle size range ($0.2 < r < 1.6$ μm) of the composite input aerosol size distributions. The result is an overestimate of the aerosol refractive index, since the routine attempts to attribute a certain amount of backscattering to aerosol size distributions that underestimate the particle size in the critical size range where the FSSP-300 data are used.

In conclusion, the TARFOX aerosol refractive index retrieval routine performs well, provided that the input aerosol size distribution data can be validated and errors in the input lidar-derived aerosol backscatter data are random. Figures 7a and 8a illustrate the results for the refractive index retrievals for case studies 1 and 12, respectively, in the form of the comparisons of the vertical profiles of the *in situ* and the lidar-derived total scattering ratio R. Figures 7b and 8b show the respective contour plots of Δ (see (4)). Note the "broadening" effect of the Δ minima in Figure 8b in comparison to 7b, which is apparently caused by the errors in the input data themselves.

3. Results of TARFOX Data Analysis

In this section we will describe the application of the methodology developed in section 2 to two TARFOX case

Table 1. Sensitivity Studies for the TARFOX Refractive Index Retrieval Scheme

Case	Description	Input Refractive Indices	Retrieved Refractive Indices	For Layer i
1	exact values of m_r and m_i	1: 1.378 - 0.00011i	1: 1.378 - 0.00011i	1: 0.000
		2: 1.547 - 0.05743i	2: 1.547 - 0.05743i	2: 0.000
		3: 1.402 - 0.00224i	3: 1.402 - 0.00224i	3: 0.000
2	rounded values	1: 1.380 - 0.0001i	1: 1.378 - 0.00013i	1: 0.008
		2: 1.550 - 0.060i	2: 1.547 - 0.05743i	2: 0.002
		3: 1.400 - 0.002i	3: 1.402 - 0.00224i	3: 0.005
3	rounded values	1: 1.378 - 0.00012i	1: 1.378 - 0.00011i	1: 0.003
		2: 1.547 - 0.05400i	2: 1.547 - 0.05743i	2: 0.007
		3: 1.402 - 0.00202i	3: 1.402 - 0.00224i	3: 0.008
4	rounded values	1: 1.390 - 0.0001i	1: 1.402 - 0.00013i	1: 0.016
		2: 1.560 - 0.0600i	2: 1.547 - 0.04626i	2: 0.004
		3: 1.414 - 0.0020i	3: 1.427 - 0.00278i	3: 0.012
5	systematic error in lidar data: +5%	1: 1.378 - 0.00011i	1: 1.402 - 0.00026i	1: 0.012
		2: 1.547 - 0.05743i	2: 1.547 - 0.03726i	2: 0.007
		3: 1.402 - 0.00224i	3: 1.402 - 0.00224i	3: 0.009
6	systematic error in lidar data: +10%	1: 1.378 - 0.00011i	1: 1.402 - 0.00013i	1: 0.020
		2: 1.547 - 0.05743i	2: 1.620 - 0.08854i	2: 0.011
		3: 1.402 - 0.00224i	3: 1.451 - 0.00278i	3: 0.015
7	systematic error in lidar data: +20%	1: 1.378 - 0.00011i	1: 1.427 - 0.00026i	1: 0.019
		2: 1.547 - 0.05743i	2: 1.620 - 0.04626i	2: 0.012
		3: 1.402 - 0.00224i	3: 1.475 - 0.00224i	3: 0.022
8	systematic error in lidar data: +30%	1: 1.378 - 0.00011i	1: 1.451 - 0.00026i	1: 0.021
		2: 1.547 - 0.05743i	2: 1.668 - 0.05743i	2: 0.013
		3: 1.402 - 0.00224i	3: 1.499 - 0.00145i	3: 0.026
9	underestimate of FSSP-300 radii: 20%	1: 1.378 - 0.00011i	1: 1.475 - 0.00061i	1: 0.033
		2: 1.547 - 0.05743i	2: 1.596 - 0.01947i	2: 0.011
		3: 1.402 - 0.00224i	3: 1.451 - 0.00278i	3: 0.022
10	random error in lidar data: ±10%, ∅=5%	1: 1.378 - 0.00011i	1: 1.378 - 0.00001i	1: 0.069
		2: 1.547 - 0.05743i	2: 1.547 - 0.07131i	2: 0.032
		3: 1.402 - 0.00224i	3: 1.402 - 0.00224i	3: 0.046
11	random error in lidar data: ±20%, ∅=10%	1: 1.378 - 0.00011i	1: 1.354 - 0.00001i	1: 0.065
		2: 1.547 - 0.05743i	2: 1.523 - 0.08854i	2: 0.057
		3: 1.402 - 0.00224i	3: 1.402 - 0.00224i	3: 0.103
12	random error in lidar data: ±30%, ∅=15%	1: 1.378 - 0.00011i	1: 1.354 - 0.00005i	1: 0.013
		2: 1.547 - 0.05743i	2: 1.499 - 0.01568i	2: 0.176
		3: 1.402 - 0.00224i	3: 1.354 - 0.00032i	3: 0.169

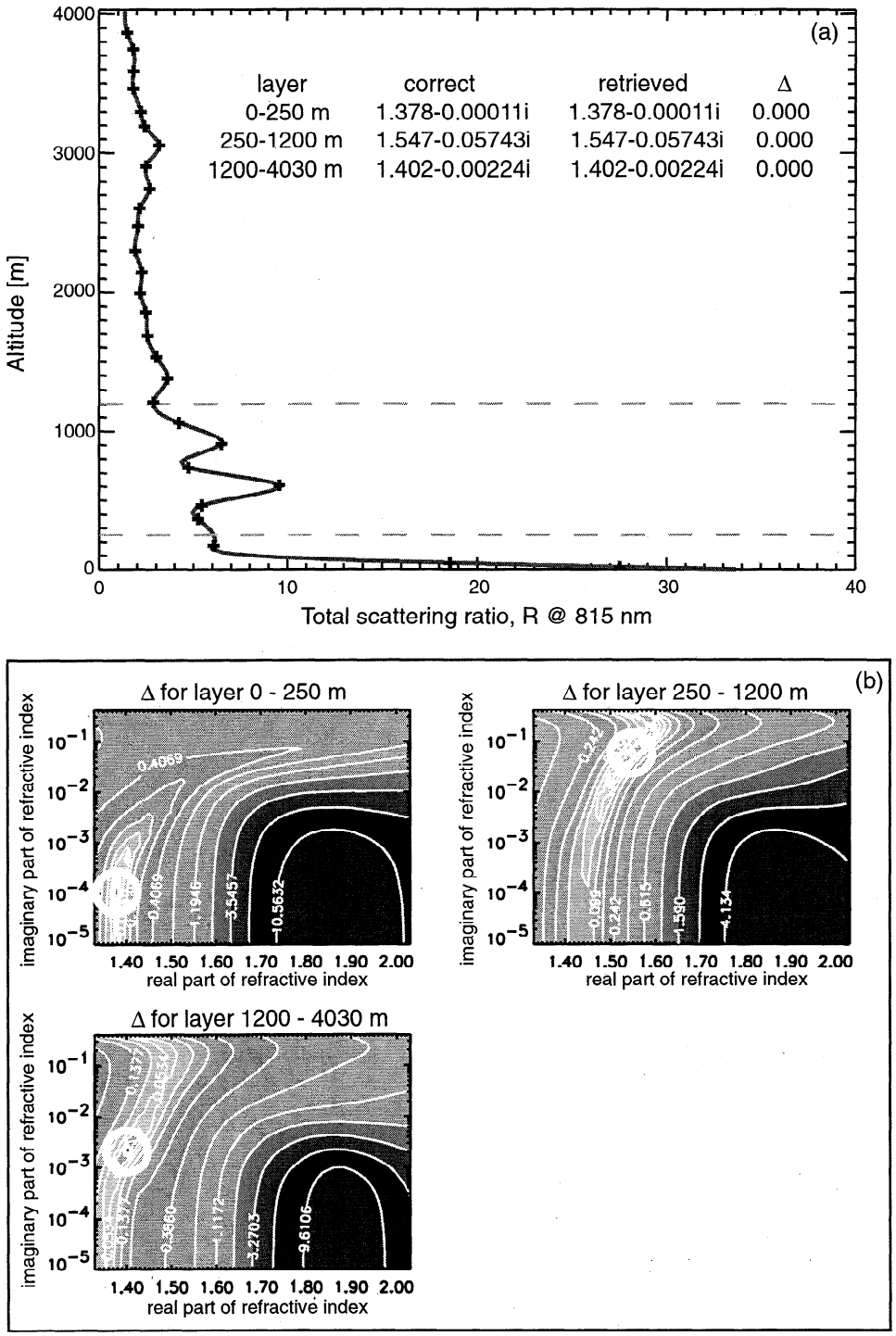

Figure 7. (a) Scattering ratio R for sensitivity study 1 (see Table 1); no errors in either the *in situ* particle size distributions or the lidar data. (b) Δ as a function of the real and imaginary parts of the aerosol refractive index for the three layers in Figure 7a. The circles mark the location of the minima in Δ, indicating the best fit aerosol refractive index for each layer.

studies on July 17 and July 24, 1996. Furthermore, we will add an additional step to our refractive index estimation technique, in which we forward calculate the aerosol optical depth in distinct layers from the *in situ* particle size distributions using the best match backscatter refractive indices and compare it to values derived from the sunphotometer measurements. This step mandates the adjustment of the *in situ* particle size distribution data to achieve mutual consistency between the different remote sensing measurements and the *in situ* particle size distribution data (in a manner described below). The additional step in the refractive index estimation scheme results in a set of particle size distribution and refractive index data, which is in agreement with both the lidar-derived aerosol backscatter profiles and the sunphotometer-derived aerosol optical depths. Thus the

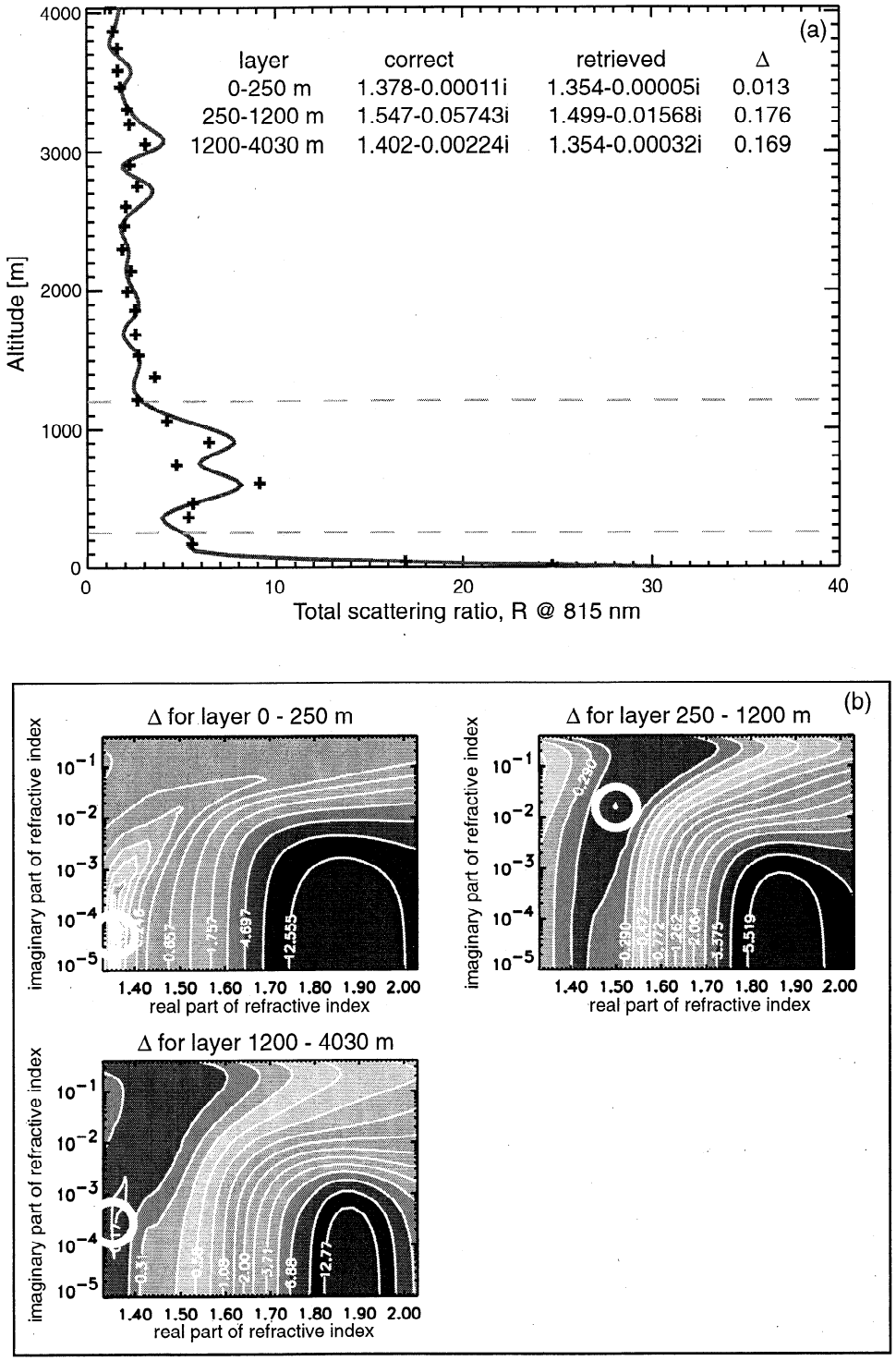

Figure 8. (a) Scattering ratio R for sensitivity study 12; a random error of ±30% in the input lidar data results in a slight underestimate of the real aerosol refractive indices (see Table 1). (b) Δ as a function of the real and imaginary parts of the aerosol refractive index for the three layers in Figure 8a. The circles mark the location of the minima in Δ, indicating the best fit aerosol refractive index for each layer.

incorporation of the sunphotometer optical depth measurements minimizes the potential for propagation of errors in the input aerosol size distribution measurements into the refractive index estimates.

3.1. Case Study 1, July 17, 1996

The TARFOX mission on July 17 was focused on vertical profile measurements by the UW C-131A coordinated with overflights by the NASA ER-2 aircraft approximately 110 km East of Wallops Island (37.7° N, 75.4° W). The ER-2 was directed to fly a racetrack pattern with 185 km legs spaced about 11 km apart. At about 18:30 Coordinated Universal Time (UTC) (14:30 local time (LT)) the flight tracks of the ER-2 and the UW C-131A crossed, with a temporal separation of less than 3 min. The UW C-131A reached that location (37.5° N, 74.2° W) at an altitude of less than 30 m and started a spiral ascent of 30 min duration. The lidar data for the comparison with the *in situ* data were collected over a latitude region of 37.51° N to 37.55° N and a longitude band of 74.14° W to 74.26° W and covered a time span of about 2 min. Because of frequent turns of the ER-2 aircraft the data needed to be screened carefully because the lidar data are less accurate when the lidar beam points off the nadir direction. Here we discarded any lidar profiles taken when the aircraft roll angle was greater than 4°.

The *in situ* particle size distribution data for this profile study are binned into 60-s averages, yielding a vertical resolution of the *in-situ*-derived aerosol backscatter profile of about 130 m, depending on the instantaneous ascent rate of the UW C-131A aircraft. Figure 9a shows the comparison of the *in situ* and lidar-derived total scattering ratios, with the best fit aerosol refractive indices indicated in text boxes. The gray shaded areas delimit the variability in the lidar scattering ratio data in terms of the maximum and minimum values during the 2 min time period used for producing the average scattering ratio curve.

The profile in Figure 9a was subdivided into three different vertical layers, based on the lidar signal, which showed a strongly backscattering surface layer to about 250 m in altitude, a boundary-type layer between 250 and 1650 m, and a free troposphere layer between 1650 and 4030 m. The altitude-averaged lidar ratio $\bar{g}$ (see equation (2)) is 67.2 sr, indicating that the assumption of 60 sr for this variable in the standard LASE lidar data inversion is reasonable for this case study. The variability in the lidar data for Figure 9a is largest in layer 2 (as indicated by the gray areas), most likely caused by inhomogeneities in the local aerosol amount and related properties.

Figure 9b shows the average difference Δ between the lidar- and the *in-situ*-derived total scattering ratios in Figure 9a as a function of the real and the imaginary parts of the aerosol index of refraction. As discussed in sections 2.5, the minima in Δ mark the location of the best fit backscatter aerosol refractive index.

Based on these estimates of aerosol refractive indices, aerosol optical depths in the three vertical layers can be calculated by integrating the aerosol extinction (calculated using the *in situ* particle size distributions) with respect to altitude. Figure 10 shows the comparison of sunphotometer and *in-situ*-derived aerosol optical depth spectra in the three distinct vertical layers indicated by the lidar profile (see Figure 9a) and for the entire profile (bottom panels), respectively. The left-hand panels in Figure 10 show the actual optical depth spectra, while the right-hand panels show the ratios of sunphotometer and *in-situ*-derived aerosol optical depths.

A qualitative inspection of Figure 10 shows that the *in-situ*-derived aerosol optical depth profiles underestimate the sunphotometer-derived values, with the largest underestimate appearing in the two lowest layers. The figure further indicates that most of the underestimate indeed stems from the two lowest layers with ratios of 1.49 to 2.15 (layer 2) and 3.0 - 4.0 (layer 1), respectively.

One possible explanation for the *in situ* aerosol optical depth underestimate could be that the retrieved "best fit backscatter aerosol index of refraction" is sensitive to aerosol particles that do not affect the aerosol extinction to the same degree. However, a difference in sensitivity between the aerosol backscatter and the extinction to the index of refraction could not explain an underestimate of a factor of 2 or more, since the aerosol extinction for the investigated particle size distributions is not that sensitive to the index of refraction. A more likely reason for the underestimate are uncertainties in the *in situ* particle size distribution measurements, either in terms of the particle number concentration or in terms of the particle size. Therefore we devised a sensitivity study that systematically investigated the importance of certain parts of the input particle size distributions for the retrieved refractive indices and the subsequent effect on the optical depth spectra comparison. In brief, the sensitivity study revealed that an increase in the particle sizes of that part of the size distributions covered by the FSSP-300 instrument ($0.2 < r < 1.6$ μm) had the desired effect of increasing the aerosol optical depth while altering the aerosol backscatter the least. The physical basis for such an underestimate of the particle size by the FSSP-300 could be related to the fact that the index of refraction of the ambient particles increasingly deviates from the refractive index of the calibration particles as the aerosols become more aqueous.

Using an iterative procedure, we determined that no assumed uniform increase in FSSP-300 particle size produced good agreement between the optical depth spectra at all levels. For example, an increase of 20% results in good agreement between the optical depth in layer 3; the FSSP-300 particle sizes in layers 1 and 2 need to be increased by 68% and 40%, respectively, to achieve agreement between the sunphotometer and the *in-situ*-derived optical depth spectra.

Since this is an iterative procedure, the particle size adjustment in turn has an effect on the refractive index retrieval from the backscatter comparison. Figure 11 shows the refractive index retrieval that is based on the adjusted aerosol size distributions and yields good agreement between the sunphotometer and the *in-situ*-derived optical depth spectra. Because there are larger particles in the adjusted particle size distributions for all layers, the real parts of the retrieved refractive indices are consistently lower than those based on the original particle size distributions in Figure 9. It is noteworthy that the refractive indices thus derived become more aqueous with decreasing altitude. The refractive index of the lowest layer is $1.33 - 0.00117i$ and increases to $1.451 - 0.00224i$ for the uppermost layer.

To give quantitative proof that the adjusted *in situ* particle size distributions and the newly estimated refractive indices yield good agreement between the two optical depth spectra, Figure 12 shows the comparison of the sunphotometer-derived aerosol optical depth spectra to the *in-situ*-calculated optical depth spectra, now using the adjusted particle size distributions. With the adjustment of the particle size in the FSSP-300 size range of 68% for the lowest, 40% for the middle, and 20% for the uppermost layer, respectively, the optical depth spectra derived from the two methods agree very well. This agreement is a

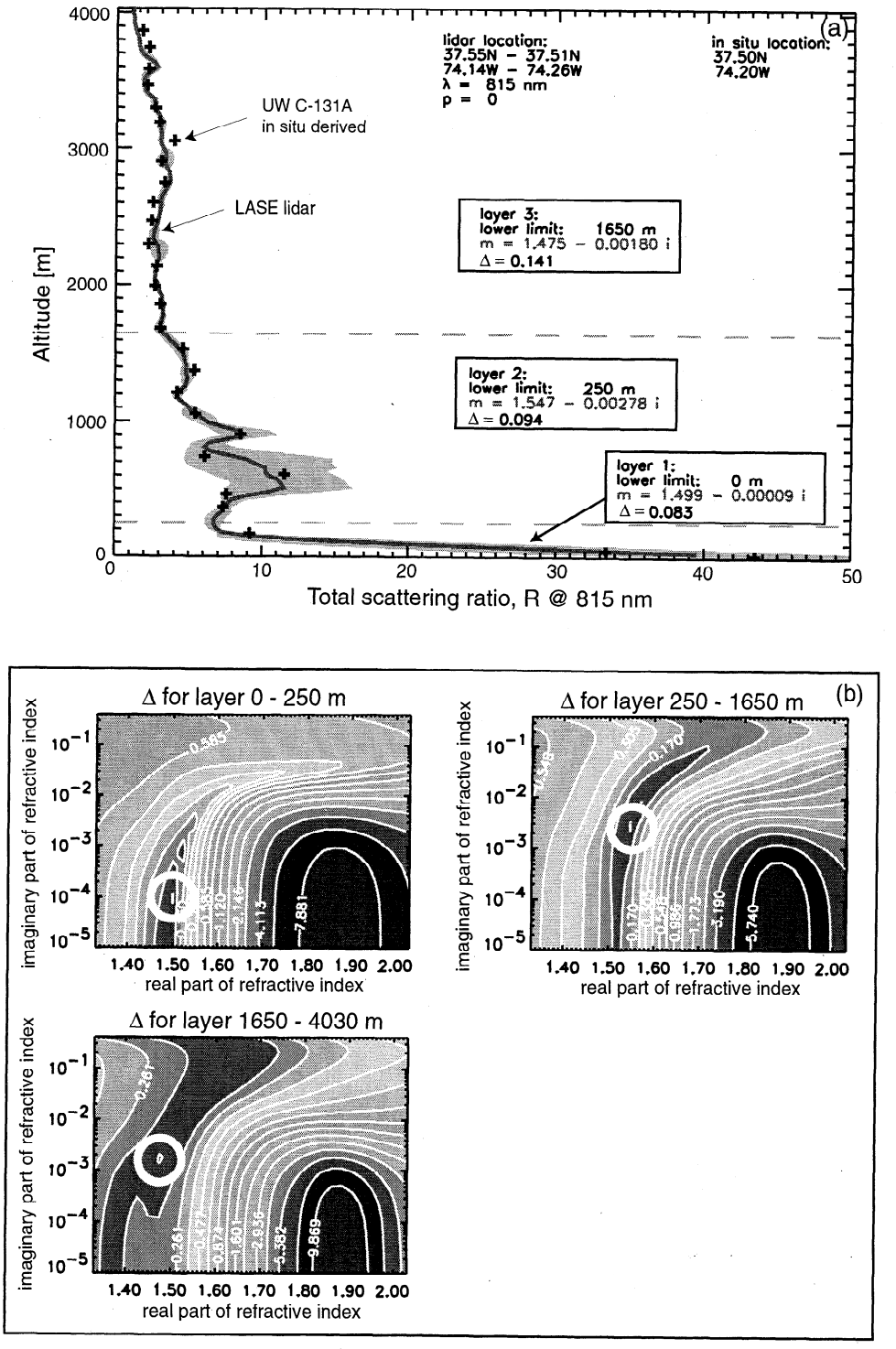

Figure 9. (a) Comparison of LASE lidar-derived total scattering ratio (solid line) and *in-situ*-derived (pluses) total scattering ratio (815 nm) for TARFOX case study 1, July 17. The *in-situ*-derived values are based on the original particle size distributions and the retrieved "best fit backscatter" refractive indices (given in text boxes). The gray shaded area denotes the variability in the archived scattering ratio data used for producing the lidar scattering ratio curve (see text). (b) Δ as a function of the real and imaginary parts of the aerosol refractive index for the three layers in Figure 9a. The circles mark the location of the minima in Δ, indicating the best fit aerosol refractive indices.

consequence of the fact that the adjustment of the *in situ* particle size distribution was performed with the goal of fitting the *in-situ*-derived optical depth spectra to the sunphotometer-derived values.

Further, the assumption that the aerosol index of refraction is constant in the wavelength region of 380 to 1020 nm (in the forward calculation of the aerosol optical depths from the *in situ* particle size distributions) is reasonable, since the *in-situ*-derived

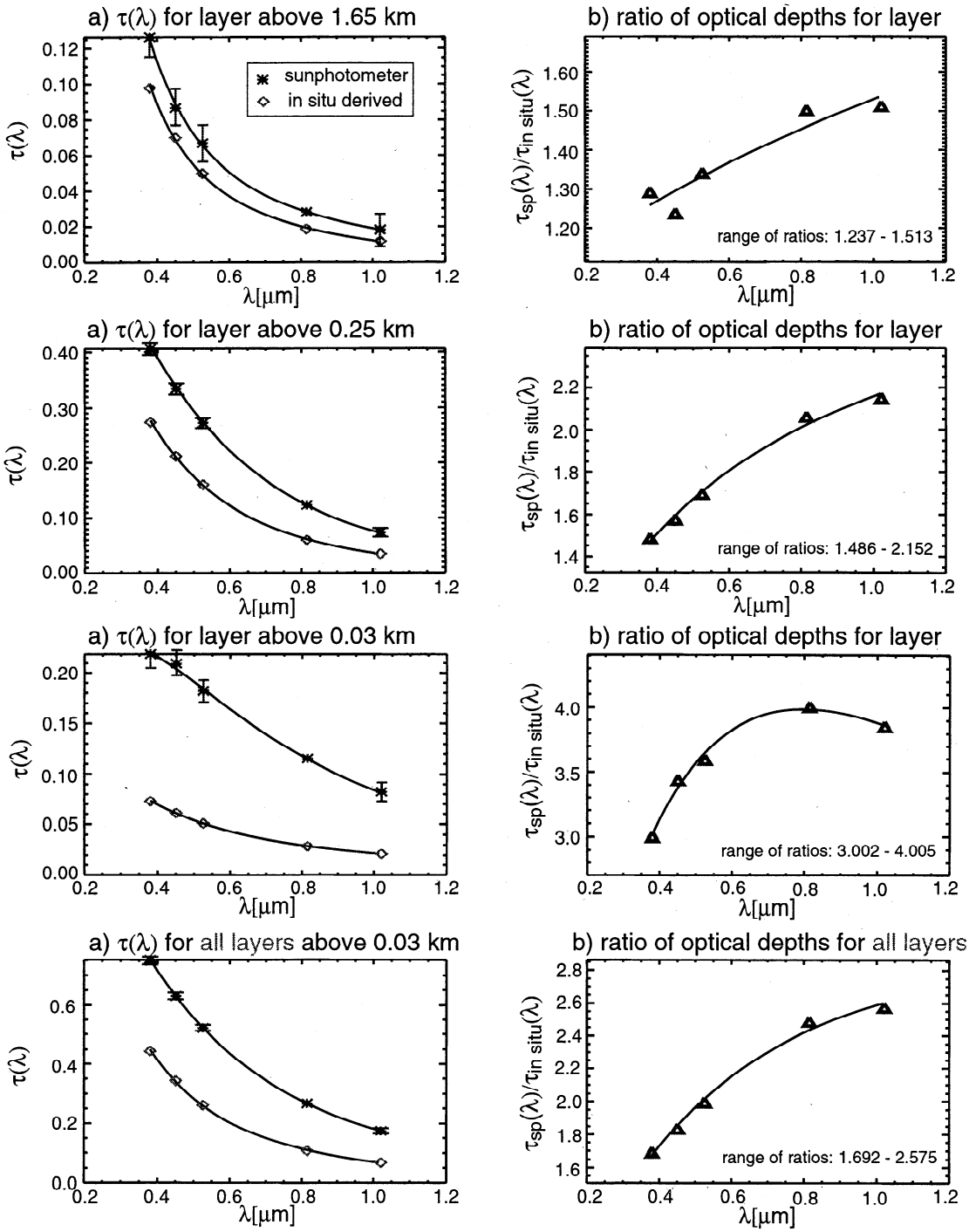

Figure 10. (a) Comparison of sunphotometer (asterisks) and *in-situ*-derived (diamonds) aerosol optical depth spectra in distinct vertical layers as indicated in Figure 9 and for the entire profile (bottom left-hand corner). (b) Ratio of the sunphotometer to the *in-situ*-derived aerosol optical depth spectra from Figure 10a also as a function of wavelength.

aerosol optical depths agree well with the sunphotometer-derived values over the entire wavelength interval.

In summary, this case study showed that the sunphotometer-derived aerosol optical depth can aid in constraining the estimate of the aerosol index of refraction. Moreover, neglecting the sunphotometer measurements would have resulted in a set of particle size distribution and refractive index data that would have underestimated the aerosol optical depth at 815 nm by about a factor of 2. Incorporating the aerosol optical depth values derived from the sunphotometer measurements results in a data set of aerosol size distributions and refractive indices, that is in accord with both the lidar aerosol backscatter measurements and the independent sunphotometer-derived aerosol optical depth spectrum from 380 to 1020 nm.

3.2. Case Study 2, July 24, 1996

The measurements for the second case study analyzed in this work took place just off the shoreline of North Carolina at 38.7° N and 74.6° W (point A). The ER-2 flew its racetrack

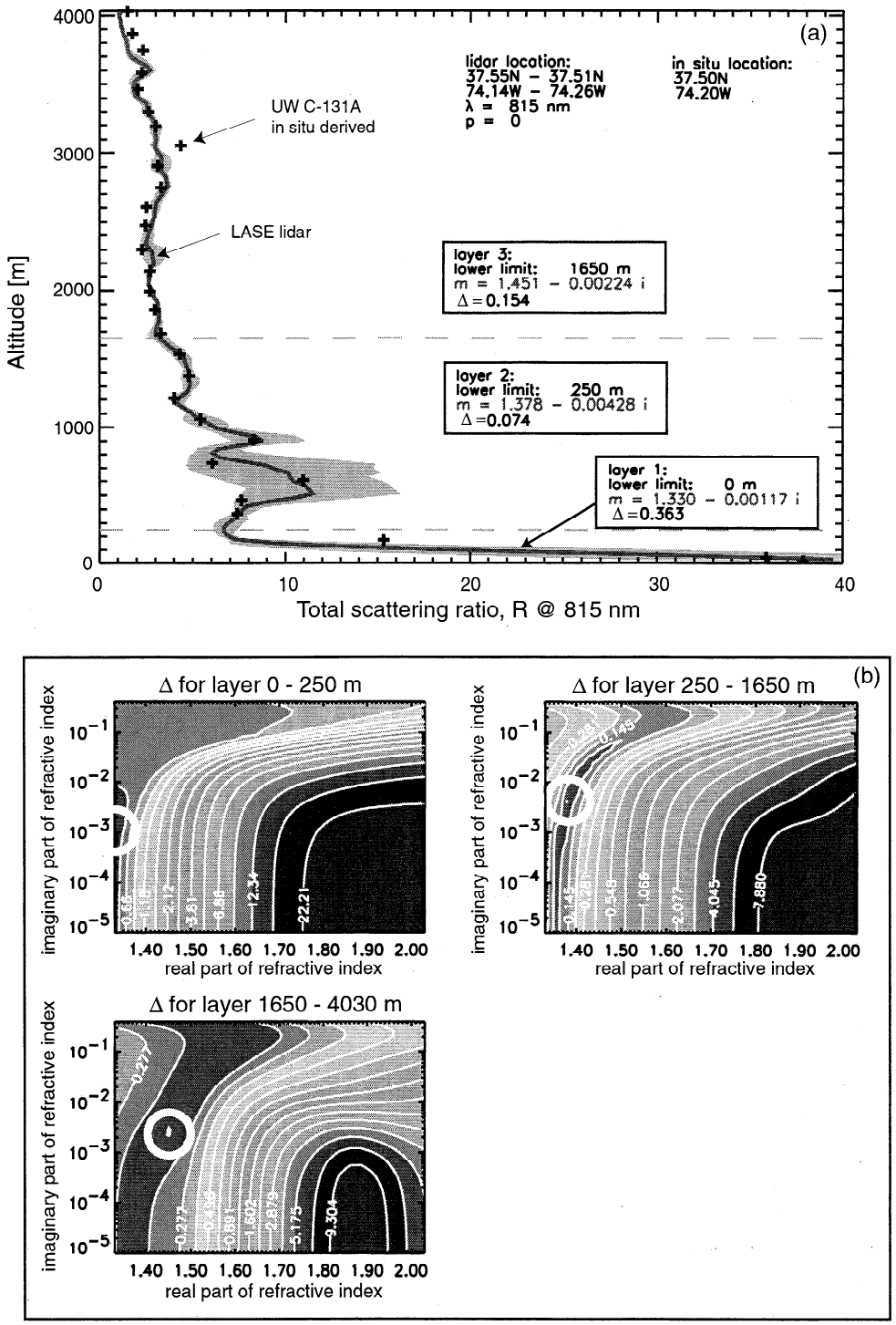

Figure 11. (a) Comparison of LASE lidar-derived total scattering ratio (solid line) and *in-situ*-derived (pluses) total scattering ratio (815 nm) for TARFOX case study 1, July 17. Here the *in-situ*-derived values are based on the adjusted particle size distributions as indicated in the text. The gray shaded area denotes the variability in the archived scattering ratio data used for producing the lidar scattering ratio curve (see text). (b) Δ as a function of the real and imaginary parts of the aerosol refractive index for the three layers in Figure 11a. The circles mark the location of the minima in Δ, indicating the best fit aerosol refractive indices.

pattern with legs of 110 km, approximately 37 km apart, but the ER-2 take-off was at 16:45 UTC, while the UW C-131A started its mission flight at 15:00 UTC. During the first part of the UW C-131A flight, a vertical profile was flown over point A. However, because of the time lag between the UW C-131A ascent and the ER-2 overflight, a refractive index estimation was not possible. The data analyzed here are from a UW C-131A ascent at about 19:00, since the flight paths of the ER-2 and the UW C-131A crossed within less than 5 min at that point and time.

The aerosol refractive index retrieval for this case study is based on LASE lidar data taken between 19:03:30 and 19:05:30,

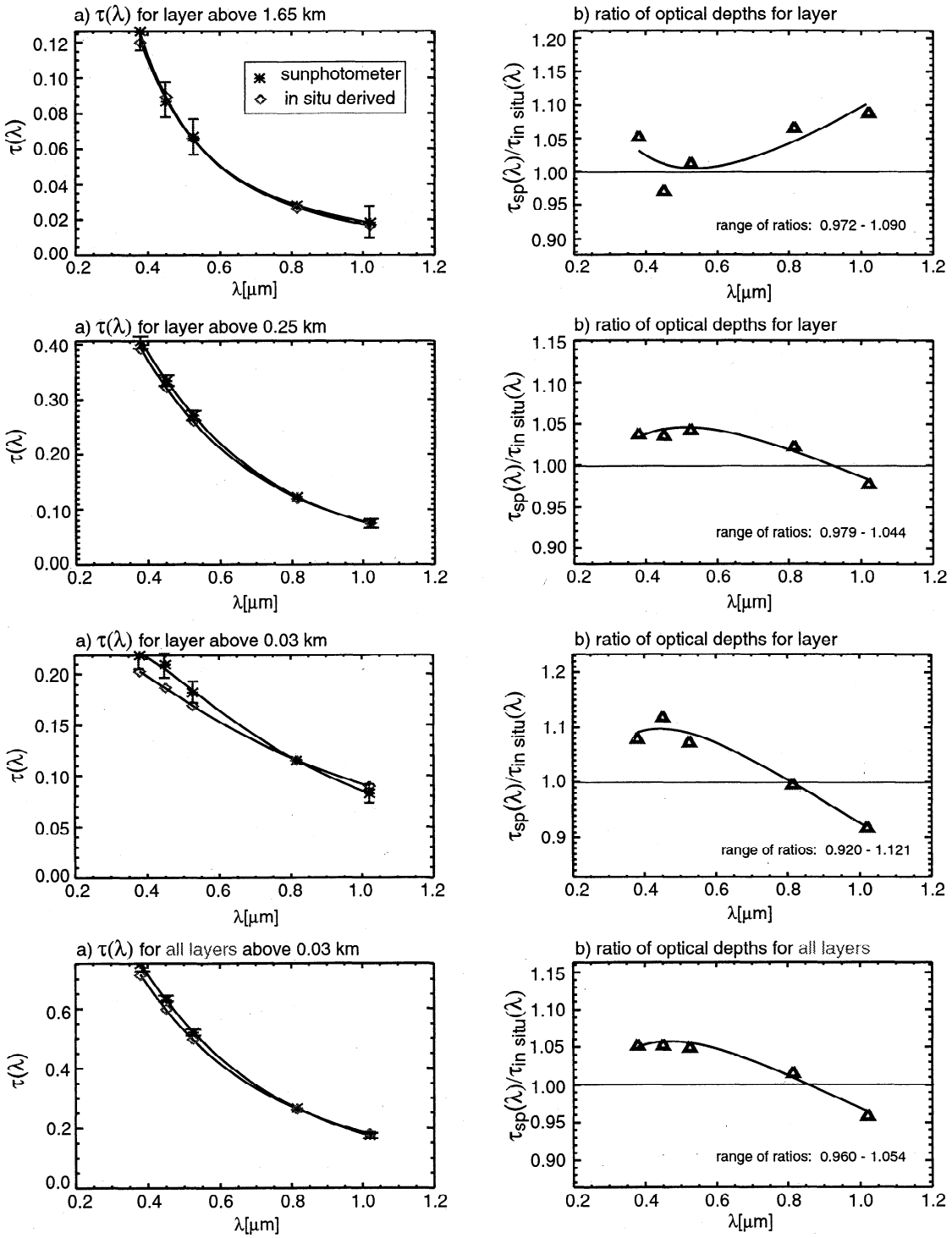

Figure 12. (a) Comparison of sunphotometer (asterisks) and *in-situ*-derived (diamonds) aerosol optical depth spectra in distinct vertical layers as indicated in Figure 11 and for the entire profile (bottom left-hand corner). (b) Ratio of the sunphotometer to the *in-situ*-derived aerosol optical depth spectra from Figure 12a also as a function of wavelength. Here the *in-situ*-derived aerosol optical depth spectra are based on the adjusted particle size distribution data, hence the good agreement.

covering the latitude region of 38.72° - 38.83° N and the longitude region of 74.44° - 74.67° W. At the same time, the UW C-131A started its ascent at 38.79° N and 74.58° W. The aerosol refractive index retrieval, based on the original particle size distribution data binned into 40-s averages, yields two layers of distinct aerosol index of refraction (see Figures 13a, 13b). The refractive index in the surface layer could not be retrieved because this layer was only about 150 m thick and contained only one 40-s average *in situ* particle size distribution. As described in sections 2.5, the refractive index estimate requires a minimum of two *in-situ*-derived backscatter values, making a refractive index retrieval in this layer impossible. Hence the lower layer in this

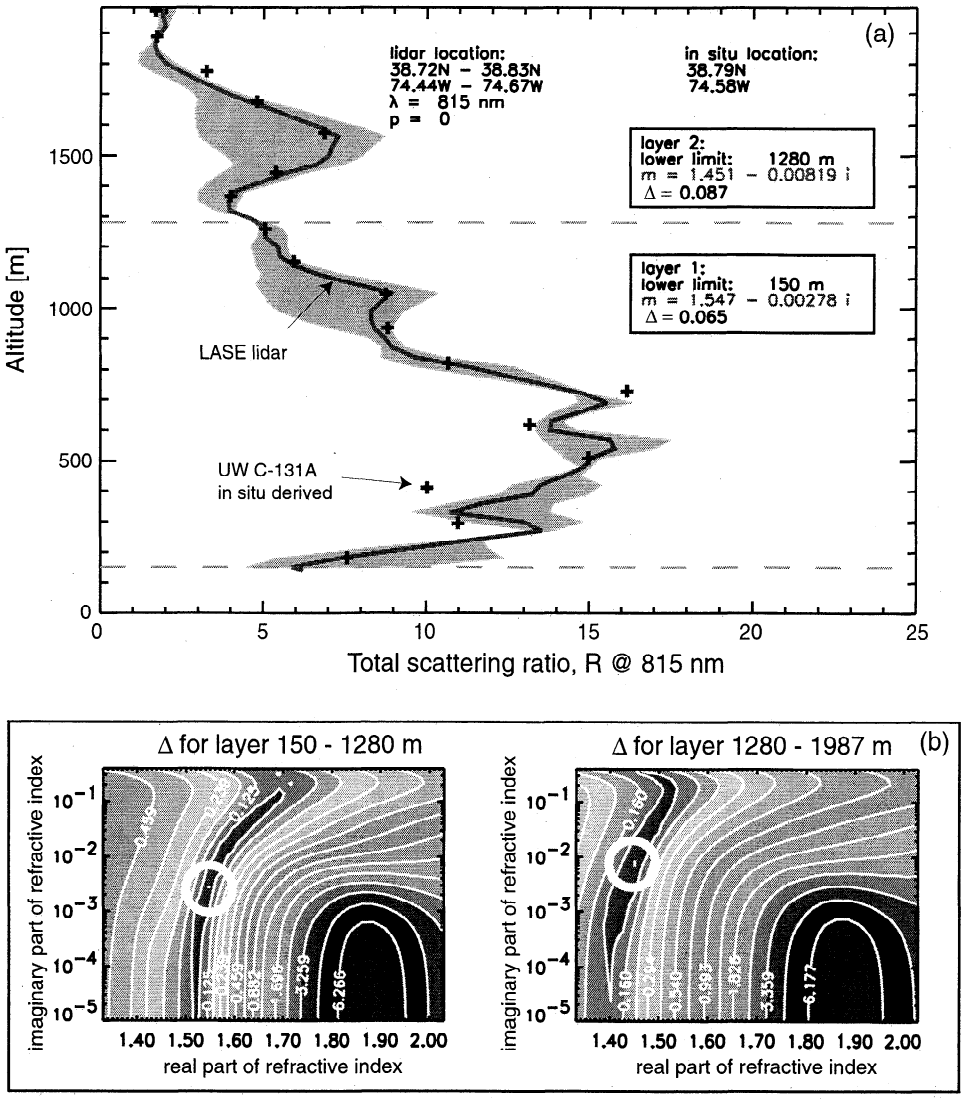

Figure 13. (a) Comparison of LASE lidar-derived total scattering ratio (solid line) and *in-situ*-derived (pluses) total scattering ratio (815 nm) for TARFOX case study 2, July 24. The *in-situ*-derived values are based on the original particle size distributions and the retrieved "best fit backscatter" refractive indices (given in text boxes). The gray shaded area denotes the variability in the archived scattering ratio data used for producing the lidar scattering ratio curve (see text). (b) Δ as a function of the real and imaginary parts of the aerosol refractive index for the three layers in Figure 13a. The circles mark the location of the minima in Δ, indicating the best fit aerosol refractive indices.

two-layer profile starts at an altitude of 150 m, yielding an aerosol refractive index of 1.547 - 0.00278*i*. The lidar data clearly show a second layer at about 1500 m. In this layer an aerosol refractive index of 1.451 - 0.00819*i* was retrieved. For this profile study, the altitude-averaged lidar ratio $\bar{g}$ (see (2)) is 47.9 sr, which is reasonably close to the standard value of 60 sr assumed in the LASE data inversion.

Figure 14 provides a comparison of the aerosol optical depth spectra as derived from the sunphotometer and the *in situ* particle size distributions in the two distinct layers shown in Figure 13. Analogous to Figure 10, Figure 14 contains the ratios of the optical depths from the two methods in the right-hand panels. The bottom two panels show the optical depth spectra and ratios for the entire profile.

In contrast to case study 1, this case study already contains a layer in which the *in-situ*-derived aerosol optical depth spectrum agrees well with the sunphotometer-derived one (layer 2, above 1.28 km). However, since most of the optical depth in this spectrum resides in the lower layer, the total profile optical depths are underestimated by 30-65%. An iterative procedure similar to the one discussed in the previous section revealed that the best fit of the sunphotometer-derived aerosol optical spectrum for the lower layer in Figure 14 could be achieved by increasing the FSSP-300 particle radii by a factor of 30%. This adjustment is smaller than the adjustment necessary in case study 1. Figure 15a shows the comparison of the scattering ratio profiles after the adjustment to the *in situ* particle size distribution data has been made, while Figure 15b shows the corresponding plots of the average difference Δ between the lidar- and the *in-situ*-derived total scattering ratios in Figure 15a as a function of the real and the imaginary parts of the aerosol index of refraction. It is noteworthy that the retrieved refractive indices for the two layers

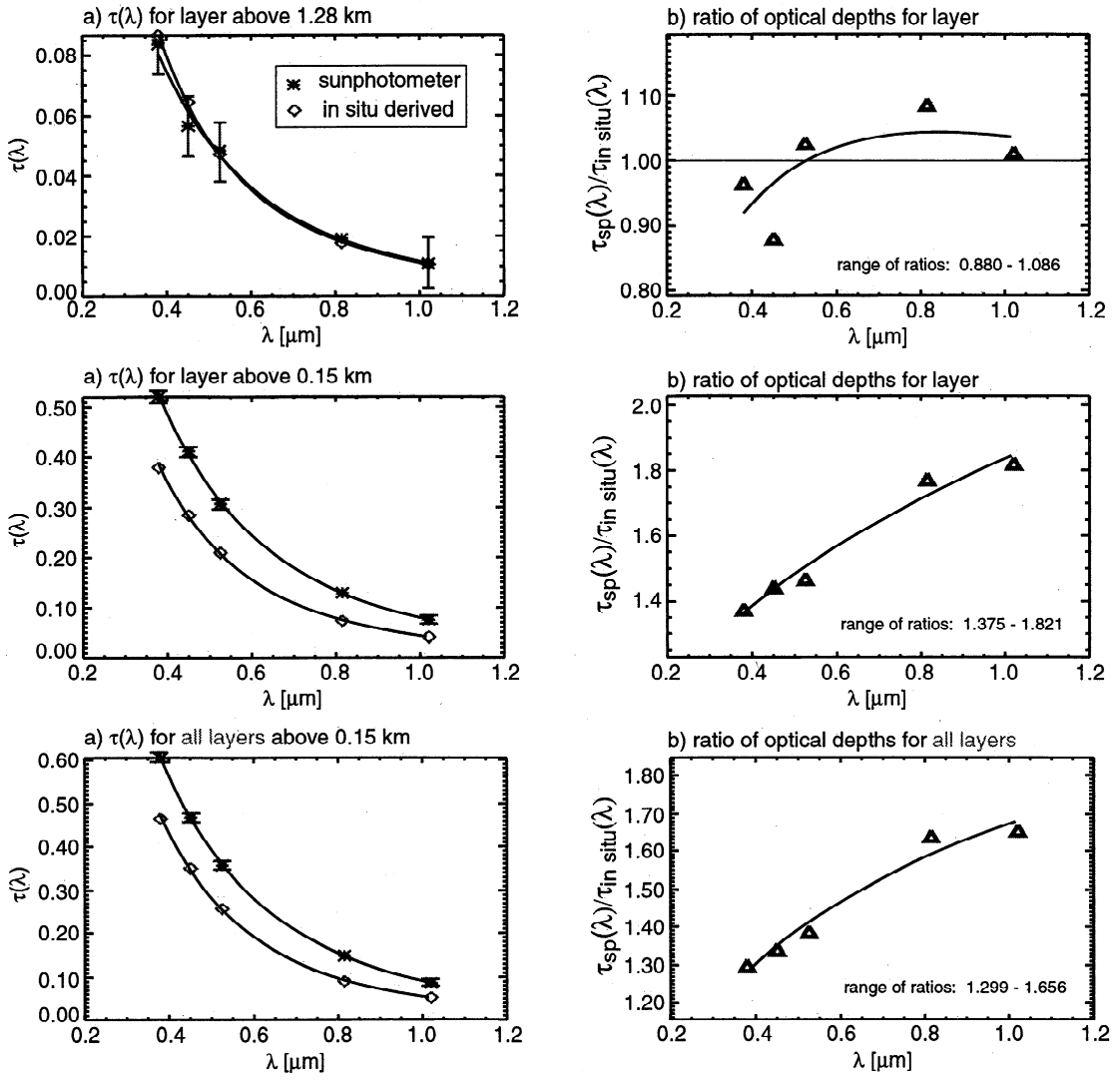

Figure 14. (a) Comparison of sunphotometer (asterisks) and *in-situ*-derived (diamonds) aerosol optical depth spectra in distinct vertical layers as indicated in Figure 13 and for the entire profile (bottom left-hand corner). (b) Ratio of the sunphotometer to the *in-situ*-derived aerosol optical depth spectra from Figure 14a also as a function of wavelength.

now only differ in their imaginary part, with $m_r = 1.451$. Figure 16 shows the comparison between the sunphotometer-derived aerosol optical depth spectra and the *in-situ*-derived ones after the adjustment to the *in situ* particle size distributions in the lower layer was performed. Now the aerosol optical depth spectra are in good agreement, as indicated by the total profile optical depth ratios between 0.96 and 1.05 (see bottom right-hand plot). Importantly, this agreement was achieved by adjusting only the aerosol particle size distribution data in the lower layer of the profile.

4. Summary of Results

A new retrieval scheme for the aerosol complex index of refraction has been developed and successfully applied to measurements obtained during two days of the TARFOX field campaign. The new technique requires the simultaneous measurements of vertically resolved aerosol *in situ* particle size distributions and coincident lidar aerosol backscatter and optical depth profiles. Basically, the technique entails two steps: in the first step, the aerosol index of refraction is estimated by matching aerosol backscatter profiles derived from our in situ measurements with those determined by the lidar, assuming that the aerosol refractive index is constant within distinct vertical layers in these profiles. In a second step, the aerosol refractive indices thus derived are tested by calculating the aerosol optical depth spectrum in the distinct layers and comparing it to simultaneous sunphotometer aerosol optical depth measurements. In the cases where the aerosol optical depths thus derived do not agree, an iterative adjustment to the *in situ* particle size distribution data is applied in such a way as to match the sunphotometer-derived aerosol optical depths. In this manner, a set of aerosol *in situ* particle size distribution data and refractive indices is derived that is in accord with both the lidar-derived aerosol backscatter profiles and the sunphotometer-derived aerosol optical depths in distinct vertical layers.

While the aerosol refractive indices in the PEM West B data analysis by *Redemann et al.* [1998a] were estimated from a set of only seven discrete refractive indices published in the literature [*Kent et al.*, 1983], the new technique considers an array of 1500

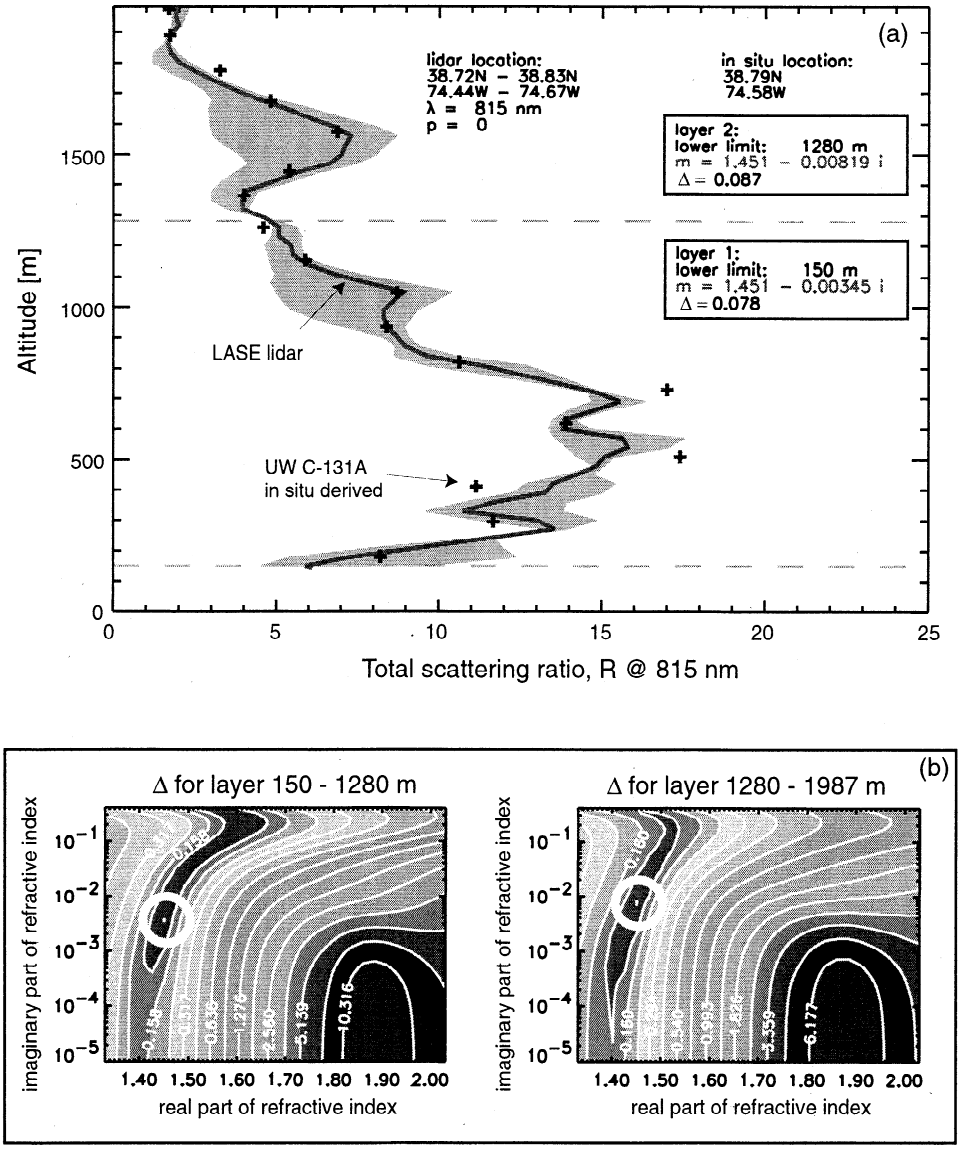

Figure 15. (a) Comparison of LASE lidar-derived total scattering ratio (solid line) and *in-situ*-derived (pluses) total scattering ratio (815 nm) for TARFOX case study 2, July 24. Here the *in-situ*-derived values are based on the original aerosol size distribution in the upper layer and adjusted particle size distributions in the lower layer, as described in the text ($r_{FSSP\text{-}300}$ + 30%). The gray shaded area denotes the variability in the archived scattering ratio data used for producing the lidar scattering ratio curve (see text). (b) Δ as a function of the real and imaginary parts of the aerosol refractive index for the three layers in Figure 15a. The circles mark the location of the minima in Δ, indicating the best fit aerosol refractive indices.

complex indices of refraction in the range of $1.33 < m_r < 2.03$ and $10^{-5} < m_i < 0.4$. Sensitivity studies showed that the new methodology estimates refractive indices reliably, provided that errors in the input aerosol size distributions and lidar data are random in nature. In particular, a minimization of calibration biases in the *in situ* particle size distribution data has been identified to be crucial for the successful retrieval of aerosol refractive indices.

The technique has been applied successfully to TARFOX aerosol measurements during July 17 and July 24, 1996. Both case studies are made possible by the coordination of the NASA ER-2 and UW C-131A aircraft flight patterns, which resulted in high spatial and temporal coincidence. Attempts to apply the retrieval scheme to a case study on July 25 failed because there was a time lapse of more than 60 min and a distance equivalent to 1° latitude between the measurements aboard the ER-2 and the UW C-131A aircraft.

The results for case study 1 (July 17, 1996) yield three horizontal layers of distinct aerosol index of refraction. For a surface layer extending from the surface to about 250 m, an aerosol index of refraction of 1.33 - 0.00117*i* was derived (RH, 80-100%), for the middle layer (250 - 1650 m) an aerosol index of refraction of 1.378 - 0.00428*i* (RH, 50-65%), and for the layer from 1650 to 4030 m a refractive index of 1.451 - 0.00224*i* (RH, 30-50%). These values were retrieved after the particle size distributions were adjusted to yield agreement between the *in-situ*-derived aerosol optical depths and the sunphotometer-derived values in these distinct layers.

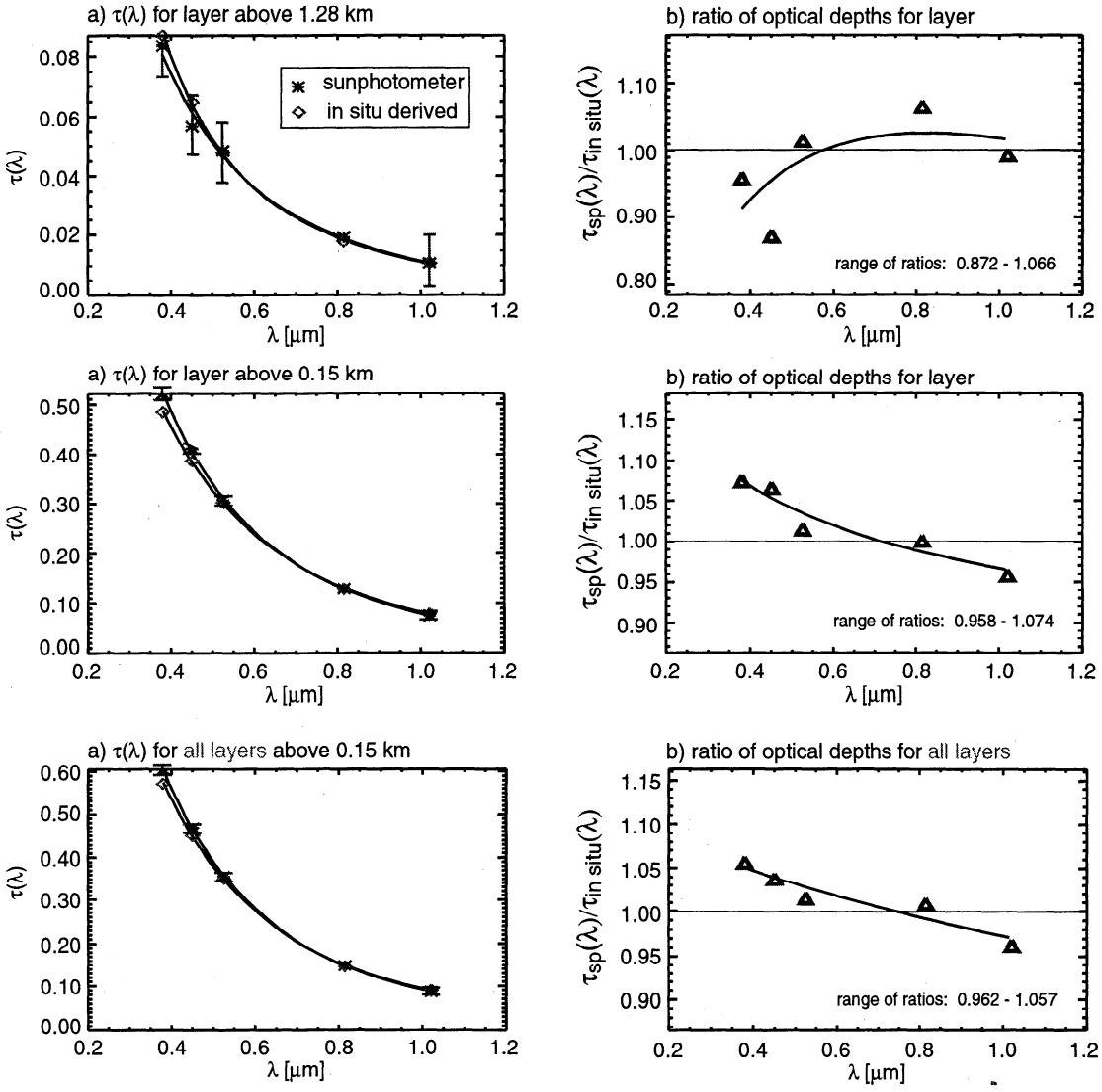

Figure 16. (a) Comparison of sunphotometer (asterisks) and *in-situ*-derived (diamonds) aerosol optical depth spectra in distinct vertical layers as indicated in Figure 15 and for the entire profile (bottom left-hand corner). (b) Ratio of the sunphotometer to the *in-situ*-derived aerosol optical depth spectra from Figure 16a also as a function of wavelength. Here the *in-situ*-derived aerosol optical depth spectra are based on the adjusted particle size distribution data, hence the good agreement.

Interestingly, the adjustment to the aerosol particle size distribution data seemed to be a strong function of the ambient relative humidity, which peaked in the surface layer (RH, 80-100%).

The systematic increase of the real part of the aerosol index of refraction with altitude may reflect the findings of *Hegg et al.* [1997] and *Novakov et al.* [1997], who show that in an average sense during TARFOX the dry aerosol carbonaceous mass fraction increased with altitude.

For the second case study on July 24, only two layers of distinct aerosol index of refraction were identified. The surface layer for this profile study was too shallow to allow the retrieval of the aerosol index of refraction. Importantly, this case study only required adjustment to the particle size distribution data in the lower layer (150 - 1280 m), where the ambient relative humidity was again higher than in the upper layer (RH, 60-70% for the lower layer versus 40-60% in the upper layer). The actual refractive indices retrieved are 1.451 - 0.00345*i* in the lower layer and 1.451 - 0.00819*i* for the layer extending from 1280 to 1980 m. The fact that the real parts of the refractive indices in the two layers are the same seems to imply that a one-layer model with one distinct aerosol index of refraction might be sufficient to explain the vertical structure in the aerosol backscatter. However, an analysis assuming just one layer (not shown here) yielded a considerable increase in the altitude-averaged difference Δ, indicating the necessity for a two-layer solution. Therefore we conclude that these measurements can best be explained with a two-layer approach, although a one-layer model might be sufficiently accurate for the calculation of an altitude-integrated aerosol property such as the aerosol optical depth.

In conclusion, the TARFOX aerosol measurements provide an overdetermined set of aerosol optical and microphysical properties. In this work, a technique has been devised that proves the compatibility of these measurements and combines them to constrain estimates of the aerosol index of refraction in distinct vertical layers. The utility of this technique depends on the

availability of well-calibrated *in situ* particle size distribution measurements. Furthermore, the coincidence of measurements from different platforms, both spatially and temporally, is essential for the inference of information from a combination of these measurements.

5. Conclusions

The TARFOX data analysis presented here suggests that the incorporation of independent, simultaneous measurements of certain aerosol optical properties (in our case, the aerosol optical depth derived from sunphotometer observations) can effectively constrain the estimates of the aerosol complex index of refraction. In particular, instrument intercomparisons in the TARFOX case studies reveal that calibration biases, present either in the *in situ* size distributions or in the remotely sensed aerosol data sets, are likely to jeopardize the validity of any conclusions drawn from these measurements regarding, for instance, the aerosol refractive index.

The work carried out here further suggests a minimum strategy for aerosol optical characterization, in which *in situ* measurements at several heights are used to determine the aerosol size distribution, while lidar and sunphotometry are used to define vertical structure and to constrain the aerosol refractive index within different layers. The utility of such a strategy is that (1) the basic measurement techniques are well founded, with reliable instrumentation available, and (2) the necessary measurements can be made sufficiently coincident both in space and in time.

The detailed results obtained here concerning the vertical structure of the aerosol microphysical and optical properties are directly applicable to the validation of satellite aerosol remote sensing schemes. As pointed out earlier, the TARFOX data set, in particular, will be useful in the interpretation of satellite-based measurements, since the combined *in situ* size distribution and refractive index data agree well with independently measured lidar aerosol backscatter profiles at 815 nm and sunphotometer-derived aerosol optical depth between 380 and 1020 nm (mostly as a result of the refractive index retrieval method). Similar correlative measurements in the future can provide powerful constraints on satellite observational systems.

In analyzing, critically and comprehensively, the range of TARFOX field data available, a new methodology has been constructed for determining the complex indices of refraction of the atmospheric aerosol and thus other important particle properties. Our approach requires that coincident aerosol observations, including lidar, sunphotometry, and *in situ* aerosol size distribution measurements, be carried out. The merit of such a multi-instrument technique is that it yields vertically resolved aerosol optical properties adequate to calculate the Earth's radiation balance with sufficient accuracy to address questions concerning radiative "closure" and anthropogenic forcing of climate [*Redemann et al.*, this issue]. The application of our new data-analysis technique to certain archived aerosol measurements might also improve our understanding of the effects that aerosols have on surface temperatures, temperature and heating profiles, large-scale circulation patterns, and the redistribution of trace species through convective processes.

Acknowledgments. TARFOX is a contribution to the International Global Atmospheric Chemistry (IGAC) core project of the International Geosphere-Biosphere Programme (IGBP). The authors would like to thank V. Brackett (SAIC) and S. Kooi (SAIC) for valuable suggestions regarding the LASE lidar data analysis. The help of D. McIntosh (Symtech, Corp.) with the preparation of this manuscript is also gratefully acknowledged. This work was funded under NSF grants ATM-96-18425 and ATM-94-12082. Support through NASA radiation science program, codes 622-44-10-10 and 622-44-75-10, and NASA grant NAGS-7675 is also gratefully acknowledged.

References

Baumgardner, D., J.E. Dye, B.W. Gandrud, and R.G. Knollenberg, Interpretation of measurements made by the forward scattering spectrometer probe (FSSP-300) during the airborne Arctic stratospheric expedition, *J. Geophys. Res.*, *97*, 8035-8046, 1992.

Bohren, C.F., and D.R. Huffman, *Absorption and Scattering of Light by Small Particles*, John Wiley, New York, 1983.

Browell, E.V., and S. Ismail, Airborne lidar measurements of tropospheric water vapor distributions, *Eos Trans. AGU*, *79* (17), Spring Meet. Suppl., S51, 1998.

Browell E.V., et al., LASE validation experiment, in *Advances in Atmospheric Remote Sensing With Lidar*, pp. 289-295, Springer-Verlag, New York, 1996.

Charlson R.J., S.E. Schwartz, J.M. Hales, R.D. Cess, J.A. Coakley Jr., J.E. Hansen, and D.J. Hofmann, Climate forcing by anthropogenic aerosols, *Science*, *255*, 423-430, 1992.

Cutten, D.R., R.F. Pueschel, D.A. Bowdle, V. Srivastava, A.D. Clarke, J. Rothermel, J.D. Spinhirne, and R.T. Menzies, Multiwavelength comparison of modeled and measured remote tropospheric aerosol backscatter over Pacific Ocean, *J. Geophys. Res.*, *101*, 9375-9389, 1996.

Ferrare, R.A., S.H. Melfi, D.N. Whiteman, K.D. Evans, and R. Leifer, Raman lidar measurements of aerosol extinction and backscattering, 1. Methods and comparisons, *J. Geophys. Res.*, *103*, 19,663-19,672, 1998a.

Ferrare, R.A., S.H. Melfi, D.N. Whiteman, M. Poellot, and Y.J. Kaufman, Raman lidar measurements of aerosol extinction and backscattering, 2. Derivations of aerosol real refractive index, single-scattering albedo, and humidification factor using Raman lidar and aircraft size distribution measurements, *J. Geophys. Res.*, *103*, 19,673-19,689, 1998b.

Ferrare, R.A., et al., LASE measurements of aerosols and water vapor during TARFOX, paper presented at the Nineteenth International Laser Radar Conference, Annapolis, Md., *NASA/CP-1998-207671/PT1*, pp. 11-14, 1998c.

Ferrare, R.A., et al., Comparison of aerosol optical properties and water vapor among ground and airborne lidars and sunphotometers during TARFOX, *J. Geophys. Res.*, this issue.

Fu, Q., and K.N. Liou, On the correlated k-distribution method for radiative transfer in nonhomogeneous atmospheres, *J. Atmos. Sci.*, *49*, 2139-2156, 1992.

Fu, Q., and K.N. Liou, Parameterization of the radiative properties of cirrus clouds, *J. Atmos. Sci.*, *50*, 2008-2025, 1993.

Hansen, J., M. Sato, and R. Ruedy, Long-term changes of the diurnal temperature cycle: Implications about mechanisms of global climate change, *Atmos. Res.*, *37*, 175-209, 1995.

Hartley, W.S., P.V. Hobbs, J.L. Ross, P.B. Russell, and J.M. Livingston, Properties of aerosols aloft relevant to direct radiative forcing off the mid-Atlantic coast of the United States, *J. Geophys. Res.*, this issue.

Haywood, J.M., and V. Ramaswamy, Global sensitivity studies of the direct radiative forcing due to anthropogenic sulfate and black carbon aerosols, *J. Geophys. Res.*, *103*, 6043-6058, 1998.

Hegg, D.A., J.M. Livingston, P.V. Hobbs, T. Novakov, and P.B. Russell, Chemical apportionment of aerosol column optical depth off the mid-Atlantic coast of the United States, *J. Geophys. Res.*, *102*, 25,293-25,303, 1997.

Hobbs, P.V., An overview of the University of Washington airborne measurements and results from the Tropospheric Aerosol Radiative Forcing Observational Experiment (TARFOX), *J. Geophys. Res.*, *104*, 2233-2238, 1999.

Jacobson, M.Z., A physically-based treatment of elemental carbon optics: Implications for global direct forcing of aerosols, *Geophys. Res. Lett.*, *27*, 217-220, 2000.

Kent, G.S., G.K. Yue, U.O. Farrukh, and A. Deepak, Modeling atmospheric aerosol backscatter at CO_2 laser wavelengths, 1. Aerosol properties, modeling techniques, and associated problems, *Appl. Opt.*, *22*, 1655-1665, 1983.

Kuze, A., and K.V. Chance, Analysis of cloud top height and cloud coverage from satellites using the O_2 A and B bands, *J. Geophys. Res.*, *99*, 14,481-14,491, 1994.

Matsumoto, T., P.B. Russell, C. Mina, and W. Van Ark, Airborne tracking sunphotometer, *J. Atmos. Oceanic Technol.*, *4*, 336-339, 1987.

Measures, R.D., *Laser Remote Sensing - Fundamentals and Applications*, John Wiley, New York, 1984.

Moore A.S., et al., Development of the Lidar Atmospheric Sensing Experiment (LASE) – An advanced airborne DIAL instrument, in *Advances in Atmospheric Remote Sensing With Lidar,* pp. 281-288, Springer-Verlag, New York, 1996.

Novakov, T., D.A. Hegg, and P.V. Hobbs, Airborne measurements of carbonaceous aerosols on the east coast of the United States, *J. Geophys. Res.*, *102*, 30,023-30,030, 1997.

Penner, J.E., R.J. Charlson, J.M. Hales, N.S. Laulainen, R. Leifer, T. Novakov, J. Ogren, L.F. Radke, S.E. Schwartz, and L. Travis, Quantifying and minimizing uncertainty of climate forcing by anthropogenic aerosols, *Bull. Am. Meteorol. Soc.*, *75*, 375-400, 1994.

Pueschel, R.F., V.R. Oberbeck, K.G. Snetsinger, P.B. Russell, G.V. Ferry, J.C. Wilson, J.M. Livingston, S. Verma, and W. Fong, Calibration correction of an active scattering spectrometer probe to account for refractive index of stratospheric aerosols, *J. Aerosol Sci.*, *12*, 992-1002, 1990.

Redemann, J., Combining remote sensing and in situ aerosol measurements for the determination of aerosol optical properties and radiative effects, Ph.D. thesis, Univ. of Calif., Los Angeles, 1999.

Redemann J., R.P. Turco, R.F. Pueschel, M.A. Fenn, E.V. Browell, and W.B. Grant, A multi-instrument approach for characterizing the vertical structure of aerosol properties: Case studies in the Pacific basin troposphere, *J. Geophys. Res.*, *103*, 23,287 - 23,298, 1998a.

Redemann, J., R.P. Turco, R.F. Pueschel, E.V. Browell, and W.B. Grant, Combining data from lidar and *in situ* instruments to characterize the vertical structure of aerosol optical properties, paper presented at the Nineteenth International Laser Radar Conference, Annapolis, Md., July 6-10, *NASA/CP-1998-207671/PT1*, pp.95-99, 1998b.

Redemann, J., R.P. Turco, K.N. Liou, P.V. Hobbs, W.S. Hartley, R.W. Bergstrom, E.V. Browell, and P.B. Russell, Case studies of the vertical structure of the direct shortwave aerosol radiative forcing during TARFOX, *J. Geophys. Res.*, this issue.

Russell, P.B., P.V. Hobbs, and L.L. Stowe, Aerosol properties and radiative effects in the United States east coast haze plume: An overview of the Tropospheric Aerosol Radiative Forcing Experiment (TARFOX), *J. Geophys. Res.*, *104*, 2213-2222, 1999a.

Russell, P.B., J.M. Livingston, P. Hignett, S. Kinne, J. Wong, A. Chien, P. Durkee, and P.V. Hobbs, Aerosol-induced radiative flux change off the United States mid-Atlantic coast: Comparison of values calculated from sunphotometer and in situ data with those measured by airborne pyranometer, *J. Geophys. Res.*, *104*, 2289-2307, 1999b.

Shettle, E.P., and R.W. Fenn, Models for the aerosols of the lower atmosphere and the effects of humidity variations on their optical properties, *AFGL-TR-79-0214,* Air Force Geophys. Lab., Hanscom Air Force Base, Mass., 1979.

Sokolik, I.N., and O.B. Toon, Incorporation of mineralogical composition into models of the radiative properties of mineral aerosol from UV to IR wavelengths, *J. Geophys. Res.*, *104*, 9423-9444, 1999.

Takamura, T., and Y. Sasano, Aerosol optical properties inferred from simultaneous lidar, aerosol-counter, and sunphotometer measurements, *J. Meteorol. Soc. Jpn.*, *68*, 729-739, 1992.

Takamura, T., Y. Sasano, and T. Hayasaka, Tropospheric aerosol optical properties derived from lidar, sunphotometer, and optical particle counter measurements, *Appl. Opt.*, *33*, 7132-7140, 1994.

Tett, S.F.B., J.F.B. Mitchell, D.E. Parker, and M.R. Allen, Human influence on the atmospheric vertical temperature structure: Detection and observations, *Science, 274*, 1170-1173, 1996.

Toon, O.B., Modeling the relationships between aerosol properties and the direct and indirect effects of aerosols on climate, in *Aerosol Forcing of Climate*, edited by R.J. Charlson and J. Heintzenberg, pp.197-213, John Wiley, New York, 1994.

J. Redemann, R.W. Bergstrom, and B. Schmid, Bay Area Environmental Research Institute, San Francisco, CA 94122. (jredemann@mail.arc.nasa.gov)

R.P. Turco and K.N. Liou, Department of Atmospheric Sciences, UCLA, Los Angeles, CA 90095.

P.B. Russell, NASA Ames Research Center, MS 245-5, Moffett Field, CA 94035-1000.

J.M. Livingston, SRI International, Menlo Park, CA 94025.

P.V. Hobbs and W.S. Hartley, Department of Atmospheric Sciences, University of Washington, Seattle, WA 98195-1640.

S. Ismail, R.A. Ferrare, and E.V. Browell, NASA Langley Research Center, Hampton, VA 23681-0001.

(Received May 12, 1999; revised October 1, 1999;
accepted October 5, 1999.)